RESEARCH ARTICLE

Key Points:
- Our measurements explicitly confirm the prediction that radio-frequency production of artificial ionospheres is practicable
- Artificial ionospheres can be created even at the midlatitude site at Arecibo Observatory
- We have confirmed 10% energy conversion-efficiency for HF radio wave to kinetic electron-acceleration at Arecibo Observatory

Correspondence to:
H. C. Carlson,
herbert.c.carlson@gmail.com

Creating space plasma from the ground

H. C. Carlson[1] [ID], **F. T. Djuth**[2] [ID], **and L. D. Zhang**[2]

[1]Physics Department, CASS, Utah State University, Logan, Utah, USA, [2]Geospace Research, Inc., El Segundo, California, USA

Abstract We have performed an experiment to compare as directly as realizable the ionization production rate by HF radio wave energy versus by solar EUV. We take advantage of the commonality that ionization production by both ground-based high-power HF radio waves and by solar EUV is driven by primary and secondary suprathermal electrons near and above ~20 eV. Incoherent scatter radar (ISR) plasma-line amplitudes are used as a measure of suprathermal electron fluxes for ISR wavelengths near those for 430 MHz and are indeed a clean measure of such for those fluxes sufficiently weak to have negligible self-damping. We present data from an HF heating experiment on November 2015 at Arecibo, which even more directly confirm the only prior midlatitude estimate, of order 10% efficiency for conversion of HF energy to ionospheric ionization. We note the theoretical maximum possible is ~1/3, while ~1% or less reduces the question to near practical irrelevance. Our measurements explicitly confirm the prediction that radio-frequency production of artificial ionospheres can be practicable, even at midlatitudes. Furthermore, that this midlatitude efficiency is comparable to efficiencies measured at high latitudes (which include enhancements unique to high latitudes including magnetic zenith effect, gyrofrequency multiples, and double resonances) requires reexamination of current theoretical thinking about soft-electron acceleration processes in weakly magnetized plasmas. The implications are that electron acceleration by any of a variety of processes may be a fundamental underpinning to energy redistribution in space plasmas.

1. Introduction, Motivation, and Logic Trail

Twenty years ago it was predicted [*Carlson*, 1987, 1993] that once ground-based HF transmitters reached the GW effective radiated power (ERP) class, the HF power densities delivered to ionospheric altitudes should be able to create an overhead ionosphere of plasma density approaching that from the Sun. Within two decades technology achieved such power densities. The first experiments to test the prediction were at high latitudes and confirmed the prediction there [*Pedersen et al.*, 2009, 2010; *Blagoveshchenskaya et al.*, 2009]. However, theory and experiment show that an important role is played there by phenomena unique to high latitudes (HF trapping, magnetic zenith effects, and multiple plasma resonances). The original prediction was based on a midlatitude measurement. The general case for HF production of ionization for "unaided" midlatitude conditions, thus, begs for test of repeatability at midlatitudes. We report here the results of such a test for generalization.

Given the above motivation, the logic flow of this paper after introductory context is to first sketch the steps key to the quantitative prediction of an HF-power-density threshold for achieving ionization rates competitive with the Sun. Of these steps, the key issue is to estimate the efficiency with which HF radio wave energy density is converted into ionospheric ionization rate. The efficiency of that conversion still cannot be quantitatively derived from theory and so needs to be experimentally estimated. This is most effectively done by dividing the problem into two components: the efficiency of conversion (wave-particle interaction) of HF energy into an accelerated suprathermal electron flux (~tens of eV) and transport of the suprathermal-electron flux to where it produces impact ionization. The latter is done by using the tools of aeronomy, including testing for self-consistency of data with theory and quantitative modeling.

The determination that plasma was being produced was based on different sets of observations at the three confirming observatories. The High Frequency Active Auroral Research Program (HAARP) confirmation was based on enhancements of optical emissions of impact-electron energy-thresholds very close (or equal) to the energy thresholds for ionization, and HF ray deviations (from ionosondes) of reflections (including reflection height reduction) attributed to enhanced ionization. The Arecibo confirmation was based on optical emission energy thresholds and suprathermal energy spectra (from incoherent scatter radar (ISR) plasma lines) exceeding ionization thresholds. The European Incoherent Scatter (EISCAT) confirmation was based
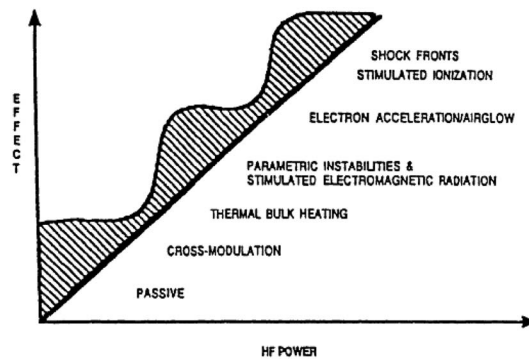
Figure 1. Hierarchy of HF heater thresholds, illustrating discontinuous changes in plasma response to continuously increasing HF power, driving plasma past higher-power-density thresholds. [*Carlson*, 1990].

on enhanced ISR ion line measured electron density. The enhanced ionization rate at Arecibo is thus not a directly measured total electron content or direct electron density profile enhancement; it is a measured enhancement of ionization production rate based on measured electron fluxes with energies above thermospheric neutral particle ionization potentials. The primary advantage of this approach is that steady state electron densities depend on the balance of three things, ionization production rate, transport of ambient ions to where they can recombine, and recombination rates; here we can directly compare the rates of ionization production alone.

Important differences between high latitude versus midlatitude electron acceleration processes are known, from both theory and observations, thus calling for quantitative test of efficiency at both latitudes. An efficiency of ~10% was estimated for HAARP in 2009. The efficiency measured at Arecibo decades before was also ~10%, hence our need to test for repeatability of this efficiency. We define and perform a definitive experiment at Arecibo, with emphasis on comparison with solar production. We devise a new way to circumvent past analysis challenges, and thus go straight to comparative suprathermal electron fluxes for HF and solar EUV drivers. This new 2015 critical experiment, repeated on separate nights, gives an efficiency of ~10%, about the same as the original experiment decades ago. This supports the original 1993 prediction. Beyond that, it further calls for reexamination of the fundamentals of the HF excited electron-acceleration processes. This suggests a generalization about the role of accelerated electrons in space plasmas exposed to large electric fields, as discussed in the text. We also point out why interpretation needs to be done within the context of kinetic theory versus earlier simpler model approximations. Also bear a distinction in mind. Electron acceleration in a simple electric field potential drop has an upper limit set by the dielectric breakdown in the media; e.g., particle accelerators require acceleration over great special scales to reach great energies. In contrast, for a plasma it is its mechanical properties and turbulence that sets the upper limit, which limit can generally be orders of magnitude greater.

2. Theoretical Context for HF-Produced Ionization at High Versus Midlatitudes

2.1. Conceptual Foundations

What happens when the strength of a time-varying electric field **E** in a plasma is increased to an arbitrarily large magnitude? We do not know. However, the research field of ionospheric modification with high-power HF radio waves has progressed greatly since its beginnings in the 1970s [*Utlaut and Cohen*, 1971; *Gordon and Carlson*, 1974]. The work in this paper relates to the high-power extreme of the HF power range of Figure 1, where stimulated ionization was proposed [*Carlson*, 1990] to occur, and a quantitative HF ERP (effective radiated power) threshold predicted [*Carlson*, 1993] for ionization production rates competitive with that from our Sun (our benchmark).

The interplay of theory and experiment has been essential to progress from the start. High-power ionospheric modification research was introduced in the open literature, by *Utlaut and Cohen* [1971]. Their findings at Plattville, CO, were based on HF heater-induced airglow, spread F, wideband field-aligned ionization structure, and wideband absorption. Work at the Arecibo Observatory soon added measured profiles of electron temperature (T_e) heating and electron density (N_e) redistribution, as well as the experimental discovery that HF power densities sufficiently great to enhance the bulk electron gas temperature have associated electric fields **E** sufficient to drive instabilities in the space plasma [*Carlson et al.*, 1972]. Increasing the plasma bulk temperature vertically redistributes bulk plasma density profiles; instabilities can lead to plasma structuring and also acceleration of a small fraction of the electron population leading to impact excitation of optical emissions in the upper atmosphere. Observations of HF excited 630.0 nm for values of T_e much below

~2700 K [*Mantas and Carlson*, 1991; *Mantas*, 1994; *Carlson et al.*, 2013] and 557.7 nm optical enhancements were common and were evidence of impact excitation by electrons of energy >4 eV.

Prevailing theory in the 1970s, however, dictated that acceleration of electrons (thermal energy ~0.1–0.2 eV) could not exceed a few eV, far below the threshold for production of ionization. An Arecibo experiment proved that theory insufficient, observing electrons accelerated to energies sufficient to produce ionization [*Carlson et al.*, 1982]. They also therein explained semiquantitatively that adding the physics of aeronomy to the plasma physics added elastic scattering of accelerated electrons, which must lead an electron to experience multiple passes through the electron acceleration region. This enabled much higher energies than prior theory, thus explaining the observation of electrons accelerated to tens of eV versus only a few eV. (HF-excited plasma waves can transfer energy to electrons by the Landau damping mechanism, with local acceleration experienced as the electrons cross cavitons, now able to have multiple passes versus a single pass through the acceleration region. This more complete physics was incorporated into the quantitative theory by *Gurevich et al.* [1985] to enable more realistic modeling.)

Ambient electrons of thermal energy ~0.1 eV at night are heated in sunlight to a few times this and up to 3 to 4 times this by deviative absorption of RF energy in HF heating experiments. Electrons in the tail of this distribution can be accelerated to ~100 times this energy by plasma instability processes. Electron energies of tens of eV are now accepted as fact based on observations with radar techniques (>25 eV by *Carlson et al.* [1982]) and energy thresholds for observed optical emissions exceeding order 10 eV (e.g., >11 eV [*Djuth et al.*, 1999; *Kosch et al.*, 2000; *Pedersen et al.*, 2003; *Hysell et al.*, 2012]) and >19 eV by *Gustavson et al.* [2006] and *Hysell et al.* [2014]. Ionization potentials for atomic oxygen O, N_2, and O_2 are respectively 13.62, 15.58, and 12.06 eV. Theory and experiment give HF suprathermal electron acceleration exceeding ionization potentials.

2.2. HF Versus Solar Radiation Energy Density for Plasma Production

The prediction that ionization competitive with that produced by the Sun could be produced from the ground [*Carlson*, 1987, 1993], projected that threshold would be passed once HF radar technology realized GW ERP levels. Quantitative prediction was based on comparison of the HF power density delivered to the *F*-region space plasma environment, relative to that from the Sun that produces our natural ionosphere. From, e.g., *Rishbeth and Garriott* [1969], an overhead Sun for average solar conditions (sunspot number ~60) leads to an electron production rate of ~10^3 cm^{-3} s^{-1} in the ionospheric *F*-region peak. This spread over ~100 km (two atomic oxygen scale heights) gives a column ionization rate of ~10^{10} ionizations cm^{-2} s^{-1} columnar rate. For ~30 eV per ionization by electron impact ionization this represents $3 \cdot 10^{11}$ eV cm^{-2} s^{-1} = $4 \cdot 10^{-8}$ W cm^{-2}. A GW ERP class HF facility would deliver ~$13 \cdot 10^{-8}$ W cm^{-2} to ~250 km altitude, i.e., comparable for an efficiency order of tens of percent.

A separate path to an equivalent answer is to use the experimental estimate of the number of auroral secondary electron-ion pairs per incident ionizing primary electron. This is typically taken as ~35 eV for incident auroral electrons [*Rees and Luckey*, 1974] reaching the *E* region. (We note that 30 eV per ion [*Carlson and Jensen*, 2015] is more realistic for the HF-accelerated electron spectrum in the *F* region.) This leads after conversion of units just as done above to a production rate observable at Arecibo, if the energy conversion efficiency from RF radiation input to accelerated electron kinetic energy output is, again, on the order of tens of percent. Since theory is not adequate to estimate the efficiency for this, one must go to experiment for an estimate. The first experimental estimate for this, ~15% [*Carlson et al.*, 1982], the sole estimate until 2009, remained till now the only estimate at midlatitudes. We summarize the key measurements for this midlatitude (magnetic dip angle ~45°) experiment in Figure 2, the key measurement in which is the PL intensity order of 1–4. This PL intensity scaled the electron energy flux.

When tests of the prediction became practicable at high latitudes, HAARP provided supporting evidence by following the same energy budget analysis of *Carlson* [1993]. HAARP with an ERP of 440 MW gave a power density of 9×10^{-8} W cm^{-2} at 200 km. A 100% efficiency, integrated over a full column, would produce 2×10^{10} ions cm^{-2} s^{-1} for an average energy per ion of 30 eV. The observation, taken as integrated over 20 km, gave 2.9×10^{10} ions cm^{-2} s^{-1}, lead to an efficiency of 10% [*Pedersen et al.*, 2009] for an assumed 20 eV/ion or 15% if assuming 30 eV/ion. Equivalently, this would be peak-production of 10^4 ions cm^{-3} s^{-1} or 2×10^5 ions cm^{-3} at the production peak in 20 s.
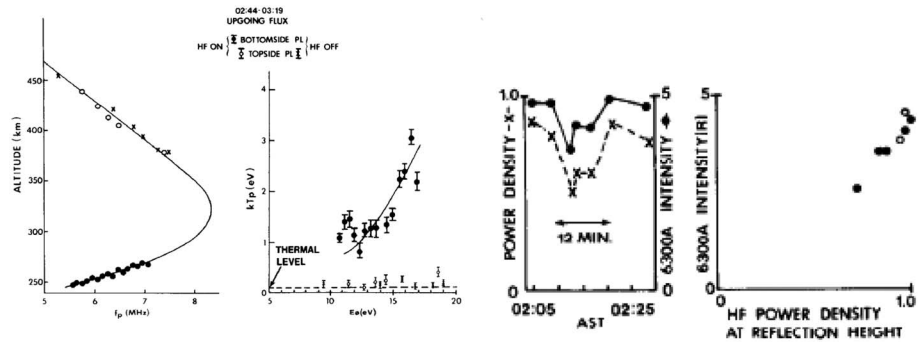
Figure 2. (left) Altitude profile of ionosphere plasma frequency (electron density), and kT_p plasma line intensity versus plasma wave phase energy E closest to equilibrium with suprathermal electrons with which energy is exchanged. (Note that topside PLs were geometrically out of the path of HF accelerated electrons.) (right) HF power density and HF impact excited 630.0 nm intensity covariation, over approximately a factor of 2 range of HF power densities, far right suggesting a threshold [*Carlson et al.*, 1982].

However, this high-latitude HAARP [*Pedersen et al.*, 2009, 2010] repeated production of ionization has been attributed to electron acceleration enhanced by the combined effects of electron gyroresonance and magnetic zenith effects [*Pedersen and Carlson*, 2001; *Gurevich et al.*, 2001; *Gurevich et al.*, 2002], including beam self-focusing on striations to amplify electron heating and electron acceleration around the magnetic zenith direction [*Gurevich et al.*, 2005; *Pedersen et al.*, 2008]. *Pedersen et al.* [2010] further published the new discovery of ionization production so strong as to produce for a time, a self-sustaining ionosphere versus production only with f_oF_2 matched to the HF.

At EISCAT, Tromsø, Norway, *Blagoveshchenskaya et al.* [2009] observed an ~25% ionization enhancement for an HF frequency near the F_2 region critical frequency and just below the third harmonic of the electron gyrofrequency. They concluded that the combined effect of upper hybrid (UH) resonance and gyroresonance at the same altitudes gives rise to strong electron heating, driving plasma striations, HF ray trapping, and HF waves reaching altitudes where they can excite fluxes of significant electron acceleration. High-latitude production of ionization is strongly enhanced by processes unique to there, yet has the same ~10% efficiency as at Arecibo, demands deeper examination.

2.3. Multiple Resonances and Striations

An O-mode HF pump wave couples through striations into electrostatic (upper hybrid (UH)) waves at the upper hybrid resonance altitude, several kilometer below the HF reflection height of the HF heating wave. UH waves propagate near perpendicular to B, their energy dissipation heating ambient electrons. Via thermal instabilities UH waves can excite artificial field-aligned irregularities (AFAIs), which can trap the UH electric field. Nonlinear stabilization of the striations [*Gurevich et al.*, 1995], self-focusing of the HF pump wave due to the density depletions within the striations [*Gurevich et al.*, 2001], and excitation of density/temperature gradient driven instabilities [*Franz et al.*, 1999] all compliment generation mechanisms. Striations are generated near the UH resonance altitude where the heater frequency is

$$f^2_H = f^2_{UH} = f^2_{pe} + f^2_{ce}$$

where f_H is the HF heater frequency, f_{UH} is the UH resonance frequency, f_{pe} is the local plasma frequency, f_{ce} is the electron-cyclotron frequency.

Experiments at HF heater frequencies near harmonics of the electron gyrofrequency

$$f_H = nf_{ce} = f_{UH} = \left(f^2_{pe} + f^2_{ce}\right)^{1/2}$$

have underscored the important consequences of HF heating at electron gyrofrequency harmonics. At high latitudes operation at the third and higher harmonics ($n =$ an integer 3 or greater) has suppressed 630.0 nm emissions, while *Djuth et al.* [2005] showed strong enhancement of 630.0, 557.7, and 777.4 nm (excitation thresholds of 1.96, 4.19, and 10.74 eV) to prove strong enhancement of ambient electron acceleration. This interlocks with strong enhancements of AFAIs produced with the Platteville, CO, HF heater at twice the electron gyrofrequency, motivation for Djuth to propose the $n = 2$ HAARP experiment. Observations include

Platteville 2–10 m irregularities tenfold increase near $2f_{ce}$, EISCAT 10 m irregularity and O(1D) minimum near $3f_{ce}$, and strong suprathermal airglow at all $n\,f_{ce}$.

Irregularities of three scale sizes transverse to B have long emerged as important: small-scale striations a few meters to tens of meters (tens of kilometers//B because of strongly anisotropic//B mobility, associated with density depletions approximately a few to 10%, separated by a few tens of meters), bunches of striations a few hundreds of meters across (at high latitudes cab self-organization into filaments a few kilometers across for pumping at magnetic zenith), larger scales of kilometers to tens of kilometers of larger involving thermal self-focusing in tens of seconds, and seen on scintillation. Other scales can emerge, e.g., a fourth scale, "super-small-scale" plasma irregularities ~0.2 m transverse by approximately a kilometer along B, have come to attention from satellite GPS observations, and have been hypothesized to be related to a four wave interaction [*Gurevich*, 2007]. Cross sections of field-aligned scattering as a function of radar frequency measured over Colorado, USA, are [*Rao and Thome*, 1974] near ~80 dB m^2 around 20–100 MHz (~15–3 m), then fall steeply to ~45–35 dB m^2 about 150–430 MHz (~2–0.7 m).

2.4. Theory in Common and Divergence at High Versus Midlatitude (MZA, UH)

Understanding partitioning of the deposition of significant fractions of radiated HF energy into the ionosphere included recognition that excitation of upper hybrid (UH) waves led to excitation of plasma striations (on scales ~10 m) found within magnetic field (**B**)-aligned structures (approximately kilometer transverse to **B**), grouped into still larger patches [see *Franz et al.*, 1999]. The logic trails of some key advances in theory between 1995 and 2001 are as follows: (1) In the starting quantitative step *Gurevich et al.* [1995] showed that a steady state of isolated striations developed during ionospheric modification by high-power HF radio waves, in which the electron gas would be heated to 2–4 times its initial thermal value, and electron plasma density (N_e) depletions would saturate at ~2–10%. (2) Because the perturbation in N_e is always negative [*Gurevich et al.*, 1997; *Kelley et al.*, 1995], this leads to parametric decay of upper hybrid waves becoming trapped inside the N_e depletions, self-focusing on striations. It is nonlinear because it feeds on itself: (as the HF pump electric field **E**p increases, it increases the depletion of N_e, further focusing the incident **E**p into further depletion of N_e, thus driving the nonlinear cycle on an increasing number of striations). (3) Focusing increases the effective **E**p, which then beyond increasing the number of striations, by producing bunches of striations [*Gurevich et al.*, 1998], large-scale structures hundreds of meters, containing meter-scale striations. (4) Because bunches (larger-scale structures) have only depleted N_e, areas of HF waves can be trapped [*Gurevich et al.*, 1999]. The trapping is most effective only for conditions where the pump HF wave is propagating sufficiently close to parallel to Earth's magnetic field **B**. (5) The geometry of the trapped region was quantified by *Gurevich et al.* [2001] as an oval region displaced toward magnetic south of the HF transmitter site. Analogous to efficiency for ionization production, HF-excited optical emission efficiency has been well documented in Figures 4 and 5 within *Pedersen et al.* [2008].

Exploration and discovery of steps (4) and (5) above were motivated by accumulating experimental indications of a basic difference between high-latitude versus lower latitude HF heating effects. Figure 3 illustrates step (4) that HF trapping is most effective only where the pump HF wave is propagating sufficiently close to parallel to Earth's magnetic field **B**.

This also likely explains otherwise puzzling early claims (pre-1970s) by Russian HF heating experiments, of ~95% HF energy absorption in their HF heating experiments.

Step (5) above further involved going well beyond self-focusing geometry, engaging the nonlinear physics of the phenomena, first in two dimensions for the concepts [*Gurevich et al.*, 2001], and then in three dimensions for more quantitative realism of comparison with experiment [*Gurevich et al.*, 2002]. Developing the theory of high-power radio waves along the magnetic field to expose the nonlinear processes of beam self-focusing on striations it further determined strong amplification of heating and particularly acceleration of plasma electrons. The dramatic enhancement of optical emission from the magnetic zenith soon became known as the "magnetic zenith effect." Experimental confirmation came right on the heels of the theory [*Pedersen and Carlson*, 2001; *Rietveld et al.*, 2003; *Pedersen et al.*, 2003; *Pedersen and Gerken*, 2005]. EISCAT was first to publish observation of an equatorial shift of the bright spot [*Kosch et al.*, 2000] without explanation, while HAARP published with interpretation (op cite), followed by rapidly repeated observational optical confirmations. Only optical photometric imagers (Autostar Suite Image Processings (ASIP)) could see the effect, so the
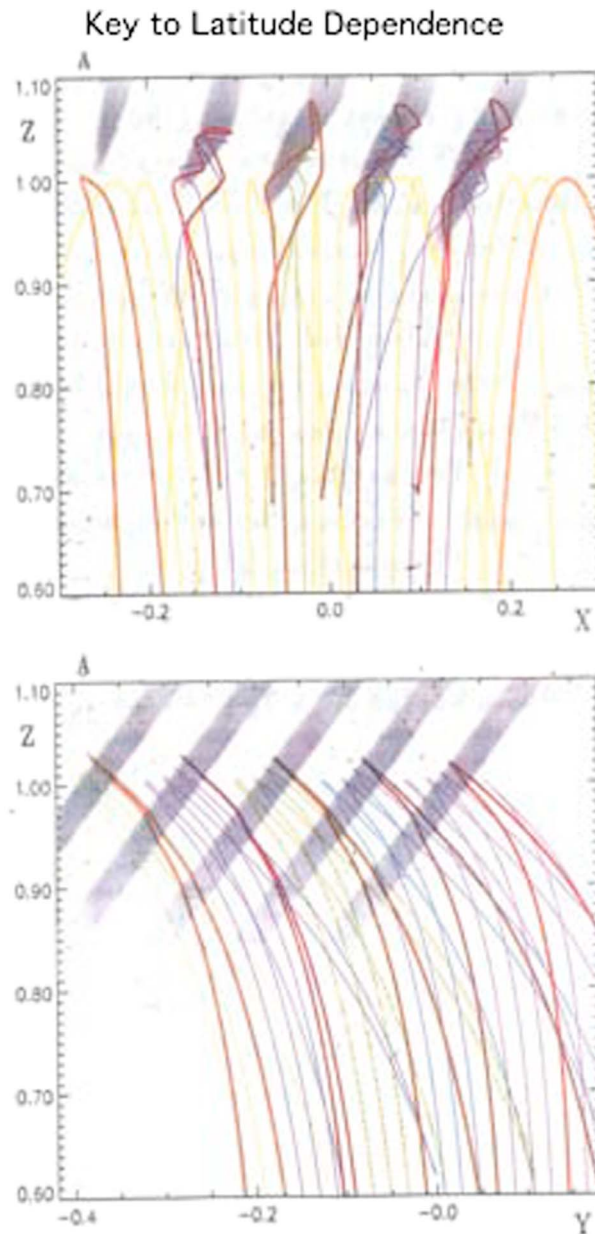
Figure 3. Central radio wave beams in magnetic meridian plane; the shaded areas show regions of depleted N_e, red rays can be trapped if propagating sufficiently close to //Earth's magnetic field **B**. (top) Ray paths for high-latitude conditions where HF waves propagate sufficiently close to parallel to **B** that bundles of rays can be trapped (e.g., HAARP, EISCAT, and Sura). (bottom) Rays are too far from //**B** to be trapped, e.g., Arecibo [*Gurevich et al.*, 1999].

explosion of publications was driven in part by the increasingly widespread fielding of ASIPs. This intersection of theory and observation was rapid and fruitful. The magnetic zenith effect [*Gurevich et al.*, 2001, 2002, 2005] has been thoroughly confirmed by many studies at HAARP, EISCAT, and Sura, as strong impact-excited airglow enhancements unique to high latitudes [*Gurevich et al.*, 2001; *Gurevich et al.*, 2002].

A further latitude effect is very strong dependence on the angle between the HF electric field **E** and Earth's magnetic field **B**. Near the HF reflection height, for a vertically propagating ordinary O-mode radio wave **E** is parallel to **B**, and conditions support Langmuir resonance and parametric instabilities. By contrast, a short distance below (typically kilometers), where the radio wave frequency is matched to the upper hybrid (UH) frequency, the radio wave **E** is perpendicular to **B**, and conditions support a very different instability. In the presence of plasma irregularities in the UH region, the HF radio wave strong electric field **E** excites UH waves, and plasma depletions trap UH waves supporting standing waves, which heat the electron gas T_e, which by expansion along **B** further reduces N_e, and further increases the depth of the irregularity depletion (thereby driving the instability). Near this UH altitude numerous plasma irregularities form in this way, and strongly elongate along **B**, expelling plasma along **B** and away from the electron-heating region. The angle of the HF **E** to Earth's magnetic field **B** thereby determines the instability growth rate and ultimate amplitude. To quantify the difference between the effectiveness of the role of this UH process at high latitude versus midlatitude, for example, at 8.175 MHz, the HF power for **E** perpendicular to **B**

at HAARP is 45%, while at Arecibo it is ~1.5%; i.e., HAARP would have 30 times the energy deposition per unit time at the UH.

Arecibo has a magnetic dip angle of ~45°, a sharp midlatitude contrast against the high latitude cases where *B* is on the order of 10° off vertical. In a nutshell, this sketches the theory of the key HF heating effects strongly amplified at high latitudes versus midlatitudes. The greatly amplified role of the UH waves just sketched the amplification of magnetic zenith angle effects, which have been well documented [e.g., *Gurevich et al.*, 2005], and electron gyrofrequency resonances. The amplification for HF operations at multiples of the electron gyro
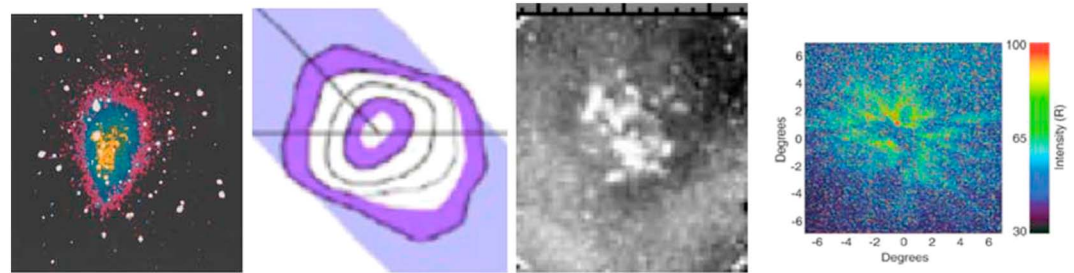
Figure 4. ASIP images of HF-excited airglow: smooth left pair Arecibo, spatially structured right pair HAARP. Typical midlatitude left pair paints the HF heater beam: far left 630.0 nm with stars shining through; left center HF-accelerated electron impact excited 777.4 nm without fine spatial structure. Typical high-latitude electron impact right pair: right center 427.7 nm and 557.7 nm showing ~1–5 km structure. The 427.8 nm maps N_2^+ ion production; 777.4 nm maps electrons of energies near or above impact ionization thresholds. (Images from left to right: 630.0 nm [*Bernhardt et al.*, 1988], 777.4 nm [*Carlson and Jensen*, 2015], 427.8 nm [*Pedersen et al.*, 2010], and 557.7 nm [*Djuth et al.*, 2005]).

harmonic frequency are also well documented [e.g., *Djuth et al.*, 2005; *Blagoveshchenskaya et al.*, 2009; *Grach et al.*, 2014]. The compound effect is major.

2.5. Experimental Motivation/Contrasts of High-Latitude Versus Midlatitude Morphology

Development of the theory just discussed above was motivated by an experimental sense of an important difference between high-latitude versus midlatitude HF heating. Consider the most visual observational contrasts. Familiar to many in the field are 630.0 nm optical images of HF-excited airglow over Arecibo by Bernhardt [e.g., *Bernhardt et al.*, 1988], which in Figure 4 here (leftmost frame in 630.0 nm) forms an overhead image approximating the HF antenna beam in the sky. ASIPs from other workers define a pattern; only the three right-hand ASIPs have to be by electron impact excitation. Midlatitude HF-accelerated suprathermal-excited airglow typically has smooth contour boundaries (structure is seen occasionally under spread *F* conditions). High latitudes typically become structured, at least within tens of seconds. Since we are addressing ionization production here, and 630.0 nm with <2 eV excitation threshold is far from ionization thresholds, the 777.4 nm ASIP over Arecibo [*Carlson and Jensen*, 2015] excited by ~10 eV can be viewed as representative of electron impact O+ production and 427.8 nm is directly imaging impact ionization of molecular nitrogen N_2^+ production.

2.6. Suprathermal Electron Transport as Framework for Experimental Test

We have noted in section 2.4 several theoretical factors unique to high latitudes that strongly favor production of HF-accelerated electrons, and in section 2.5 several morphological phenomena discriminating high-latitude versus low-latitude responses. Yet following the same budget analysis as *Carlson* [1993] at Arecibo, *Pedersen et al.* [2009] at HAARP derived an ionization rate (column-integrated production rate of $3 \times 10^9 \, cm^{-2} \, s^{-1}$) corresponding to consumption of essentially the same ~10% of the available HF power at the center of the HAARP beam. That these efficiencies are comparable demands careful examination of to what extent the Arecibo efficiency observations is repeatable.

We find that the most effective way to do this is to decompose the problem (of conversion of HF energy into ionization production by suprathermal electrons) into separable plasma physics and aeronomy components: (1) propagation of HF energy to region of electron acceleration, (2) conversion of HF radio frequency energy into kinetic energy of an electron flux for impact ionization, (3) transport of suprathermal electrons from source to the region of impact ionization production, and (4) impact ionization of O^+, O_2^+, and N_2^+.

Figures 5 and 6 facilitate visualization of this. Figure 5 coordinates are altitude versus latitude in the magnetic meridian plane. In the Arecibo observational optical data in Figure 5 (left), the red 630.0 nm emission peaks just below the height of HF reflection. The green 557.7 nm emission peaks slightly lower with to its slightly higher excitation energy threshold. The 777.4 nm emission peaking here as violet penetrates still deeper into the thermosphere (order a neutral scale height). The vertical and horizontal scales are defined by the displacement of the ASIP images of the three emission lines, within the context of the geometry of the Earth's magnetic field line **B** (dip angle 45°). Figure 6 models suprathermal penetration
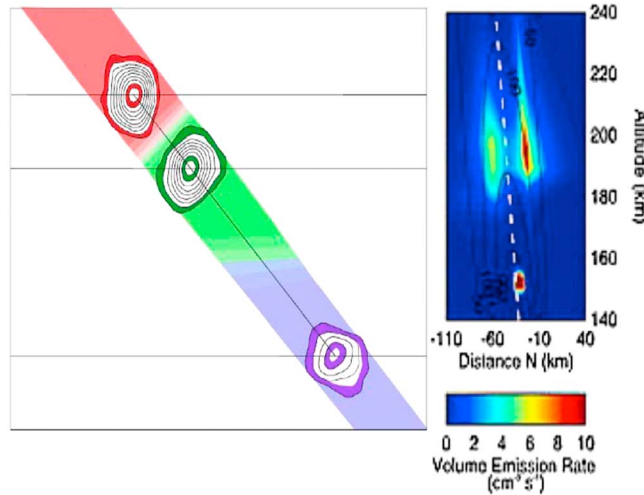
Figure 5. Side view of HF-accelerated impact excited optical emissions: (left) Arecibo 30 s combined line contours of intensity of three optical wavelength: red 630.0 nm O(1D); green 557.7 nm O(1S); violet 777.4 nm OI(3 s-p). (right) HAARP color-coded only 557.7 nm volume emission rate with 210 s combined tomographic. Both in magnetic meridian plane, north to the right, altitude vertical (HAARP axes as labeled), line at off-vertical angle is magnetic field line (Arecibo ~45° dip). Left: *Carlson and Jensen* [2015]; right: *Pedersen et al.* [2010].

quantitatively. Figure 5 (right) using data from HAARP is a tomographic construction from 5577 nm optical images. The main emission is from near the height of HF reflection, while the peak near 150 km illustrates the discovery by *Pedersen et al.* [2010] that at sufficiently high HF power, HF production of ionospheric plasma reduces the height of reflection itself. At Arecibo the ionization production is too weak to significantly reduce the height of HF reflection.

Figure 6 from a model calculation shows altitude profiles of soft electron impact optical emissions and ionization production for an HF-accelerated electron source region near optically thick conditions (near 250 km here).

This background gives us the framework to test for the efficiency we seek.

3. Experimental Test on 11 November 2015

The new nighttime PL data were collected and processed for simultaneous up/down Doppler-shifted PL echoes (respectively downgoing/upgoing suprathermal electrons) in the energy range detectable by the radar wavelength at Arecibo (usually <25 eV at night). We used coded long-pulse data-taking software [*Sulzer*, 1986] with a vertical Arecibo Observatory (AO) line feed to get an antenna gain of 18°K/J (the Gregorian has a sensitivity of 12°K/J at zenith angles below about 18°), a 430 MHz transmitter power of 1.3 MW, and two filter bandwidths of 5 MHz upshifted/downshifted by 3.0–8.0 MHz from 430 MHz. The ISR antenna gain, transmitter power monitoring, and calibration pulse were used to place an absolute scale on the PL intensity. The currently upgraded system can get detections in ~10 s with ~1 kHz and 300 m resolution (several orders of magnitude better than the fraction of an hour and 100 kHz BW filter resolution of *Carlson et al.* [1982]).
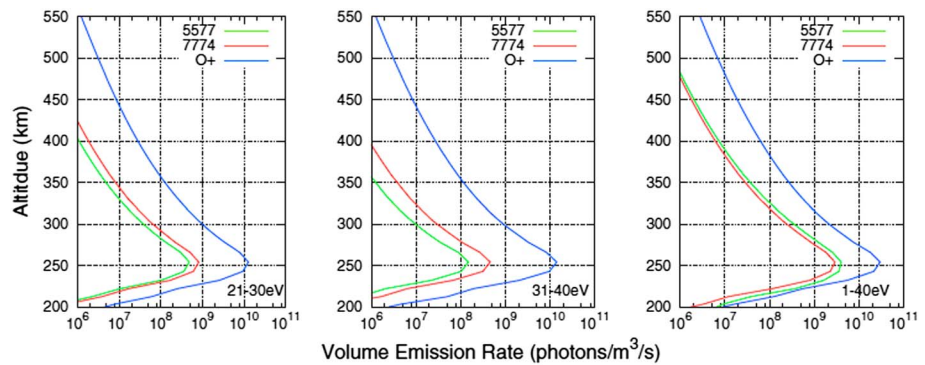

Steady State Optical Emission for Electron-Flux Source at 254 km

Figure 6. Model calculation of electron impact emission rates at 557.7 nm (4.2 eV threshold), 777.4 nm (10.7 eV threshold) and ionization rate of O^+ (threshold 13.6 eV) (green, red, and blue color-coded lines). Profiles are for 10 eV energy bins as labeled 21–30 eV, 31–40 eV primary electrons, plus an integral including secondary electrons 1–40 eV. The net contribution of secondary electrons is variable depending strongly on local electron density [*Carlson and Jensen*, 2015]. A significantly higher source altitude, in an optically thin region, would be more analogous to soft aurora electrons [*Strickland et al.*, 1983].

The data collection mode, hardware system, and software as reported in *Carlson et al.* [2015] were used during these HF heating experiments at Arecibo PR (November 2015). This was the first HF heating campaign since September 1998 when Hurricane George destroyed the field-of-dipole HF heating facility near the north coast of Puerto Rico. Arecibo HF heating experiments have been conducted in 1970–1979 with an HF feed over the 1000' dish, 1980–1994 and 1997 to September 1998 with a "Tromsø-like" field of HF dipoles near the north coast of PR east of the town of Arecibo, and now starting October 2015 with HF double-bounce from dipoles just above the dish-surface up to secondary reflector back down to the dish and up out into the ionosphere.

We present here for the first time, direct comparison of HF-produced suprathermal electrons versus solar EUV-produced electrons. Data collection was in local darkness, with a sunlit magnetically conjugate hemisphere, so the fluxes of solar-produced photoelectrons are incoming from the conjugate hemisphere. *Mantas et al.* [1978] have shown that the steady state flux from the conjugate hemisphere builds up to about 1.5 times the initial upgoing so-called "escape" flux from a local sunlit hemisphere.

For the observations taken during these first HF heating experiments with the new HF heating facility, on 11 November 2015 we heated at 5.095 MHz, offset from the nominal 5.1 MHz to keep HF sidebands out of the required PL receiver band pass. The observing mode was similar to the AO world day, but with data taking tailored to the experimental objectives much as reported in *Carlson et al.* [2015]. A major difference was in the geometry, where the PL data were collected by the Gregorian feed offset just outside the edge of the conical volume subject to intense directly driven instability echoes. The HF half power beam width (3 dB) at the HF 5.095 MHz frequency used in this experiment is ~10°. However, the threshold for excitation of strong PL echoes from instabilities directly excited near the HF reflection height, is much closer to the edge of the HF beam first null (nearly twice the half-power BW). The line feed was used in vertical to monitor the overhead ion and PL signal, including direct sensing of the instability-excited intense PL signal. To avoid any risk of intense instability echoes leading to distortion of very weak PL enhancements due to suprathermal electron fluxes (produced by these HF instability processes), we avoided an overhead ~20° full conical volume, looking at a zenith angle of 10.5° south (or north) with the Gregorian. The edge of intense PL instability-excited ISR echoes was found and verified by initially moving the Gregorian feed back-and-forth across the boundary, then parking beyond it for data-taking. For south looking, any variable HF refraction puts the HF heater beam farther from the sampled volume.

Observation were made starting pre-local-sunset through ~22:00 UT. Times of sunset on 11 November were local solar zenith angle (SZA) 0° 17:48 AST, civil twilight −6° 18:11 AST, nautical twilight −12° 19:03 AST, and astronomical twilight −18° 19:03 AST. Thus, for the PL results we report here near 19:30 AST, no suprathermal electrons could be produced locally by the Sun. We chose 19:30 AST specifically, as the time of conjugate SZA 90°, so for the observed PL, $kT_p \gg$ thermal damping $\gg kT_p$ self-damping. The T_e enhancement by the HF (on/off cycle) measured only a few 100 K, so there was negligible PL damping (f_m) by thermal electrons at these phase energies.

The diagnostic ISR beam probes a volume near but outside that illuminated by the HF beam, as indicated in Figure 7 and verified as described below. Figure 8 shows the PL intensity profile data that will be the focus of this paper. It is immediately obvious that the PL intensity between about 250 and 320 km is stronger with the HF transmitter on than when off. This enhancement is not the HF instability-enhanced PL, orders of magnitude stronger [*Carlson et al.*, 1972; *Kantor*, 1974], but driven by HF suprathermal electrons.

The 2015 AO sensitivity is so greatly improved that during this integration time the conjugate SZA changes by less then 1°. During the 1 min from 19:28:46–19:29:46 AST the weak PL intensity is enhanced only by photoelectrons (pe) from the conjugate hemisphere. The PL intensity is rather uniform above 320 km, below which collisions with increasing neutral density increasingly extinguish the incoming pe flux. Section 3.1 below shows that the PL intensity is proportional to the pe flux under the observing conditions we have chosen (for stronger pe fluxes in full sunlight this is not the case [*Carlson et al.*, 1977]). The HF transmitter turns on sufficiently before the 1 min from 19:30:16 to 19:31:16 AST, to bring the added HF-accelerated electron flux component to quasi steady state (we omit the initial 0.25 min here). By contrast, for this minute the PL profile intensity and thus the pe flux is visually seen to be virtually independent of altitude down to ~250 km. The only difference in conditions is that turning the HF transmitter on adds an HF-accelerated
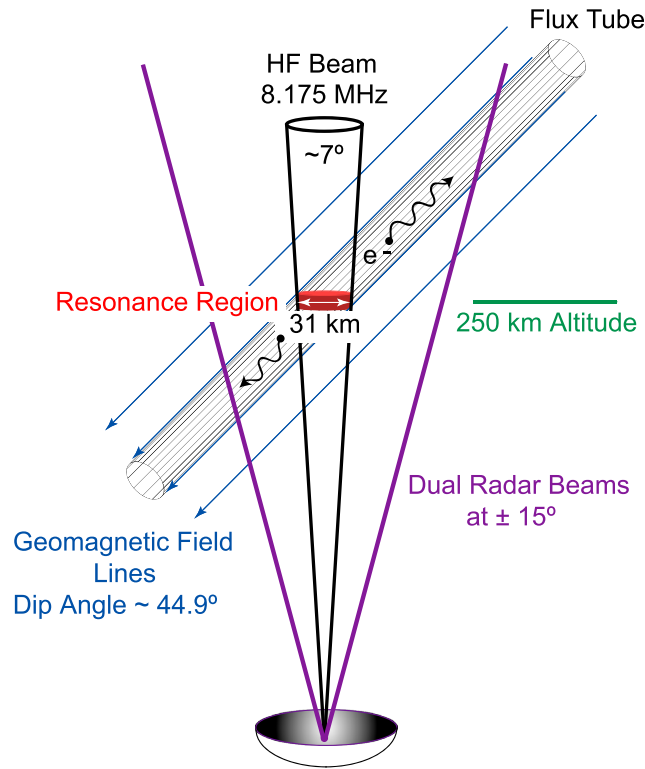
Figure 7. Representative Arecibo Observing Geometry, available as of November 2015, illustrated for 8.175 MHz. Observations here were with line feed vertical, Gregorian looking 10.4° north, and HF at 5.095 MHz (corresponding to ~10° HF beam). The region from which HF-accelerated suprathermal electrons escape is shown in red; the cylinder of magnetic flux tubes confining them is shown in grey.

suprathermal electron flux to an otherwise unchanged pe background. This thus shows by simple direct visual inspection that the HF-accelerated flux is comparable to the solar-produced incoming conjugate pe. Section 3.1 quantifies this simple visual image inspection, with much greater precision, using detailed sophisticated quantitative computer analysis sketched below.

With the HF off, Figure 8 (top) shows PL enhanced only by the conjugate sunlit hemisphere (no local Sun after local sunset, but conjugate sunlit as it is winter). Local penetration of the conjugate-source photoelectrons experiences attenuation/backscatter in the local hemisphere near and below ~300 km, as evidenced by the PL trace (sampled here from 440 km down) visibly weakening in Figure 8 as it approaches ~300 km. Figure 8 (bottom) only a minute later would look just the same if the HF transmitter were not on, but with the HF transmitter switched on, it adds additional suprathermal electrons, going up and down away from the thin HF acceleration (HF suprathermal source) region. A fraction of these HF-accelerated electrons are backscattered while streaming up/down along **B** from their thin source region to excite PLs all along **B**. The ISR can detect them only where its line-of-sight beam intersects the cylindrical bundle of magnetic field lines tracing to the HF-accelerated electron source region (the shaded bundle of flux tubes in Figure 7).

3.1. Plasma Line Measurement Technique

To quantify this we must invoke the theory underlying the PL technique. Thermal tail electrons are dependent on T_e, which in the dark night ionosphere is order 0.1 eV. The tail electrons excite Langmuir waves through the electron Landau damping process, with these waves subsequently attenuated by the same electron Landau damping process [e.g., *Perkins and Salpeter*, 1965; *Yngvesson and Perkins*, 1968—henceforth YP; *Fremouw et al.*, 1969]. This gives rise to the so-called thermal plasma line. Suprathermal electrons also excite Langmuir waves via the Landau damping process: $v_e \sim v_\varphi = \frac{f}{r} \times \lambda$, where v_e is the suprathermal electron velocity, which is slightly above v_φ, and f_r is the Langmuir frequency defined below:

$$\omega_{r\pm}^2 = \omega_{pe}^2 + \sin^2\theta \ \omega_{ce}^2 + \frac{3k_\pm^2 \kappa \ T_e}{m_e} \quad (1)$$

where $\omega_r = 2\pi f_r$, $\omega_{pe} = (n_e e/\varepsilon_o m_e)^{1/2}$, and ω_{ce} are the electron plasma frequency and the electron cyclotron frequency, respectively; n_e is electron concentration, e is electron charge, ε_o is the permittivity of free space, m_e is electron mass, θ is the angle between the radar line of sight and the geomagnetic field **B**; $k_\pm = 2\pi/c [f_o + [f_o \pm \frac{f}{r})]]$ is radar wave number corrected for wave propagation downward (+, upshifted Doppler) and upward (−, downshifted Doppler) [e.g., *Showen*, 1979]. Under nighttime conditions the second and third terms in (1) account for only 2% each of the f_r value. The energy of the suprathermal electron that excited the Langmuir wave follows as $E_\varnothing = \frac{1}{2} m_e v_\varnothing^2$. For example, $f_{r+} = 6$ MHz yields an $E_\varnothing$ of 12.6 eV (upshifted plasma line).
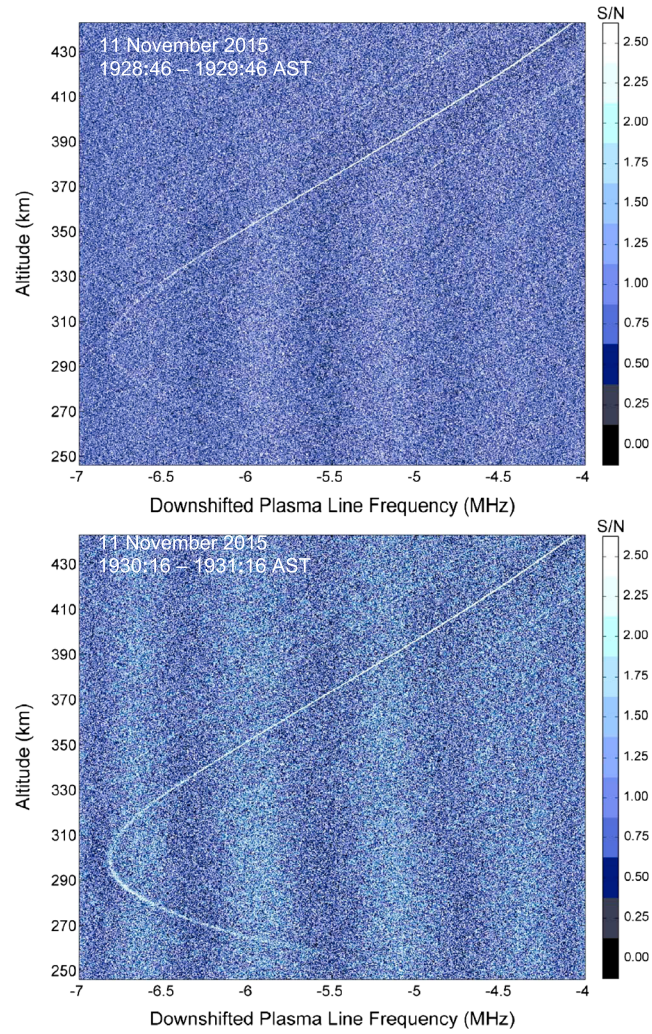
Figure 8. Arecibo observations of PL intensity profiles 240–430 km on 11 November 2015, in total local darkness, and near 90° conjugate SZA. Background downshifted plasma line profile resulting from only photoelectrons (upper) and a corresponding profile with the HF beam on (lower). The downshifted plasma line detects suprathermal electrons traveling up geomagnetic field lines. The upper profile intensity (HF transmitter off) fades near and below ~300 km as collisions extinguish penetration of conjugate photoelectrons (pe). The lower profile (HF transmitter on) shows near constant PL intensity down to ~250 km, due to an additional HF-accelerated suprathermal electron flux comparable to the incoming conjugate solar flux. Ionospheric reflection of the HF beam occurred at 249 km.

The absolute Langmuir wave energy (also listed as eV but not to be confused by $E_\emptyset$ in eV) is given in YP, repeated here in equation (2):

$$\kappa T_p = \kappa T_e \frac{f_m(E_\phi) + f_p(E_\phi) + \chi}{f_m(E_\phi) - \kappa T_e \frac{df_p(E_\phi)}{dE_\phi} + \chi} \tag{2}$$

where f_p is the one-dimensional velocity distribution of the suprathermal electrons measured along the radar wave vector and expressed as $E_\emptyset$, f_m is a modified one-dimensional velocity distribution of the ambient electrons (including the geometric effects of increased electron Landau damping due to the Arecibo radar line of sight relative to **B**), and χ provides for excitation and damping of plasma waves by the collective effects of electron-ion collisions. The geometric effects of radar line-of-sight angle to the magnetic field are detailed in YP and enhance PL damping at low-phase energies as illustrated in the Figure 1 within *Carlson et al.* [1977]. The quantities f_m and χ can be readily calculated from the measured values of T_e, n_e, the geomagnetic field strength **B**, the angle between the radar wave vector and **B**, and radar wavelength. The challenges in
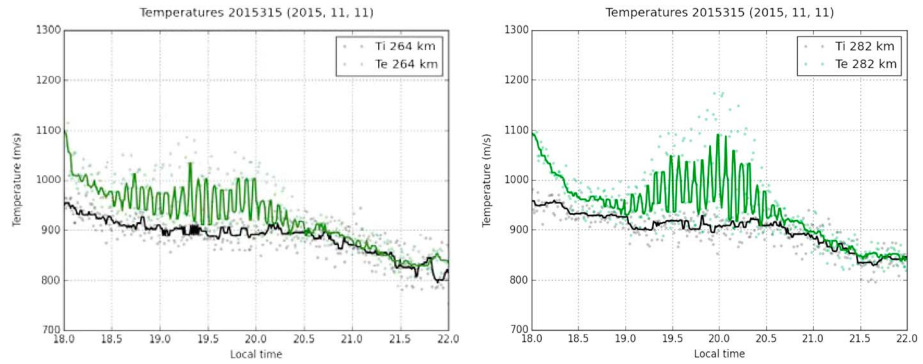
Figure 9. T_e and T_i at 228 km are 840 K $\pm$ ~10 K between 19:30 and 20:30 AST on 11 November 2015. A median filter was applied to the data (green, T_e, and black, T_i, continuous curves) to reduce the scatter in the measurements. Through 19:30 the HF-heated electron gas temperature T_e is heated by $<$200 K above T_i, taken to be very nearly T_n, both near 900 K. The 5 min HF on/off cycle is quite obvious in T_e. The fluctuations in T_i are representative of the nominal statistical error bars on the gas temperatures. These data are from the first AO heating campaign after the AO HF facility was destroyed in September 1998 by Hurricane George.

deriving suprathermal fluxes by the PL technique have been discussed by *Cicerone* [1974]; a solution for the solar produced photoelectron situation has been proposed by *Carlson et al.* [1972] by introducing modeling constraints on photoelectrons. Here we circumvent these issues as described below.

Physically, suprathermal electrons streaming through the ionosphere generate emissions of Langmuir waves via Landau damping (daytime ionospheric *F*-region thermal electrons are typically ~1000–3000 K or order 0.1–0.3 eV; the suprathermal electrons we address here are typically within the range of approximately several to 100 eV). Thermal electrons produce Langmuir waves by the same Landau damping process (several eV electrons then from the tail of the Maxwellian distribution), but with much weaker wave amplitudes and PL intensities. The PL signal intensity is proportional to the energy in these waves, in turn controlled by those electrons spending sufficient time near the same phase region of a plasma wave train to exchange wave-particle energy. Thus, the plasma wave intensity depends on the electron velocity distribution function.

The geometric effects of radar line-of-sight angle to the magnetic field are detailed in YP and enhance PL damping at low-phase energies as illustrated in the Figure 1 within *Carlson et al.* [1977]. The quantities f_m and χ can be readily calculated from the measured values of T_e, n_e, the geomagnetic field strength **B**, the angle between the radar wave vector and **B**, and radar wavelength. However, at frequencies greater than ~5 MHz at AO, B does not play a significant role because of the large gyroradii of the supathermal electrons. The challenges in deriving suprathermal fluxes by the PL technique have been discussed by *Cicerone* [1974], a solution for the general solar-produced photoelectron situation offered by *Carlson et al.* [1977] by introducing geophysics-based estimates of the suprathermal electron spectra. The complications addressed in the latter two papers are circumvented by our next step as described here below leading to equation (3).

In equation (2) we see that while the suprathermal electron flux f_p excites plasma waves, its phase energy gradient d$E_\emptyset$ also self-damps the waves. However, as illustrated in the Figure 2 within *Carlson et al.* [1977], the damping rate (for conditions below 25 eV for pe as well as HF-accelerated suprathermals) is near 2 orders of magnitude lower than the excitation rate. Here we choose a time near conjugate SZA ~90° for our HF-excited flux-efficiency experiment, for which time the pe flux arriving from the conjugate hemisphere is sufficiently weak that the self-damping term is negligible. For the T_e experienced this night T_e is ~900 K and beyond an energy of ~10 eV the thermal Maxwellian term f_m is negligible relative to the electron-ion frictional drag term χ. For these conditions, we can use the solution introduced by *Carlson et al.* [2015], where equation (2) reduces to equation here (3) below, using the ratios of kT_p/kT_e for a good linear approximation of the weak HF-accelerated suprathermal electron fluxes.

$$kT_p(E_\phi) = kT_e\left[f_p(E_\phi) + \chi\right]/\chi \tag{3}$$

Equation (3) can then be solved simply linearly for f_p, given measurement of kT_p and T_e.
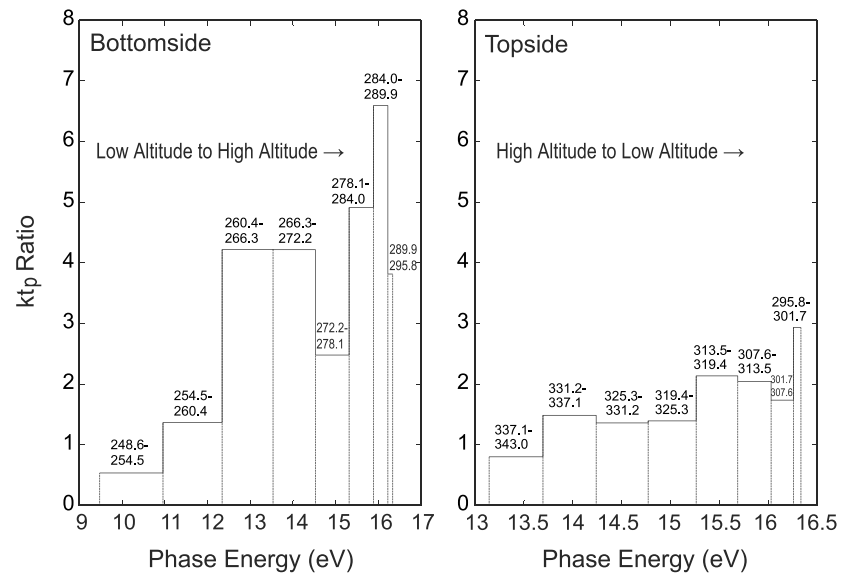
Figure 10. Ratio of suprathermal electron intensities measured with the HF on versus off. Absolute PL intensity values in units of kT_p are used for the ratios. Spectral data were fitted over 6 km altitude intervals. Major intensification is observed in the bottomside ionosphere; on the topside significant enhancement is evident only up to 320 km. At higher altitudes the 6 dB HF beam width does not map up along B into the narrow radar field of view.

3.2. New Measurement of HF-Excited PL Intensity and Efficiency of HF Conversion

The data here in Figures 8 and 9 present first new measurements of HF-induced suprathermal electrons, made during initial tests/operations of the new HF facility at AO in November 2015. The HF ERP was ~75 MW, and the frequency of the modifying HF wave was 5.095 MHz. Figure 8 shows two coded long-pulse plasma line measurements, one immediately before the HF beam was turned on and one after turn-on. The intensity ratios are shown in Figure 10. The Gregorian feed was used for the measurements and positioned at 10.5° zenith angle, geomagnetic south (in the direction parallel to **B**). Ninety percent of the 430 MHz power (1.5 MW = 100%) was directed to the Gregorian, and 10% was delivered to the line feed, which was pointed vertically. The immediate objective of the line feed measurements was to determine the resonant HF-enhanced plasma line height, but ultimately they contributed much more than that. In the future more data will be acquired, interpreted, and modeled at both 5.1 MHz and 8.175 MHz as part of the proposed project. Performance of the Arecibo HF facility is expected to extend in the near future to ~200 MW ERP when operations are available at 8.175 MHz.

For analysis software we used a revised version of the *Mantas* [1973, 1975] first principles ionosphere model to interpret the suprathermal electron results and deduce the suprathermal electron spectrum. The model includes photoelectron production for daytime studies along with improved estimates of solar photon fluxes obtained from the Extreme Ultraviolet Variability Experiment program [e.g., *Woods et al.*, 2012]. All model calculations are 2-D. The software is modular in nature and is written in Lahey Fortran. Reconstituted and updated Mantas modules [*Mantas et al.*, 1975, 1978] also exist for electron transport and thermal balance. Although other excellent photoelectron-focused models are in use, we elected to update the Mantas model because it alone went the next several critical steps to convert the photoelectron/suprathermal fluxes into the ground-based measurable of kT_p versus E_ϕ. One must recall that in contrast to in situ satellite or rocket measurements, these ground-based observations require analysis involving integrals converting 3-D fluxes into kT_p projections.,

A key focus here is to emphasize transparency in both relative comparison of solar- versus HF-produced suprathermal electron fluxes and how we estimate the efficiency of conversion of HF radio wave energy into suprathermal electron kinetic energy leading to impact ionization of thermosphere constituents. That has driven our selection of HF power (~75 kW), and observation time to have a natural pe flux source of comparable intensity and relatively free of solar-emission-line structure for relatively smooth flat spectra near 20 eV (near electron-impact-ionization thresholds for thermosphere constituents). The PL intensities and estimated
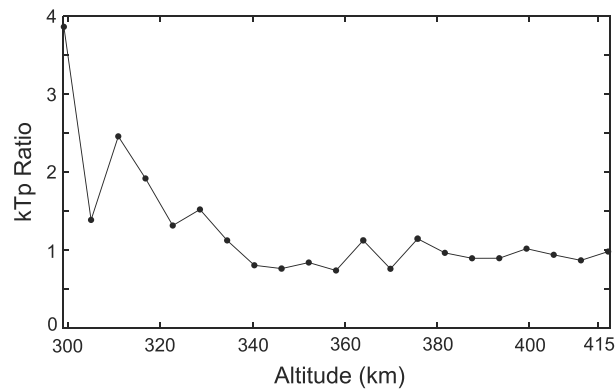
Figure 11. kT_p/kT_{pe} ratio across edge of HF beam, falls to 1.0 outside the edge of the "cylinder" within which magnetic flux tubes confine the HF-accelerated "beam" of suprathermal electrons. Figure 10 sketches the geometry of this cylinder in grey.

fluxes of suprathermal electrons below confirm the presence of these selection criteria aimed at reducing self-damping of plasma waves by the HF flux and by the pe flux during the solar versus HF flux comparison period.

In Figure 10 we show the PL intensities (imaged in Figure 8), fully quantitatively computer-processed and calibrated for presentation in units of kT_p/kT_e. T_e was measured with a precision of $\pm \sim 10$ K, and in the relevant altitude range was found to be in the narrow range ~900–1100 K (Figure 9), which values so low as to drive minimal change in thermal damping. This T_e temperature enhancement $< \sim 200$ K contrasts with T_e heating values up to 3000 K or more under other conditions. This greatly facilitates achieving our goal here, with transparency as relates to Figure 8, and quantitative rigor as relates to Figure 10. It gives high precision to defining the electron-ion frictional drag term χ in equations (3).

Figure 10 shows PL intensities measured between 249 to 343 km, an altitude range >90 km spanning bottom side to topside F region. How much of this is within the volume affected by the HF heater? Figure 7 shows the nature of the geometry, with the ISR line of sight adjacent to the cone of HF illumination. Where that cone intersects the surface of the altitude of HF reflection is slightly above the acceleration (suprathermal source) region. The "circle" of that intersection defines a cylindrical surface within which the HF effects are initially confined. Figure 11 shows the PL intensity ratio across the edge of the instability-impacted volume and exemplifies the sharpness of the instability-cutoff at the edge of the HF beam, in support of our observed sharp cutoff near 320 km.

The Figure 10 ratio of the PL intensity with the HF on versus the HF off can be noted to decrease from ~4 in the near bottomside F region to ~2 in the near topside (over a distance approximately a neutral scale height). Recall that the downgoing conjugate pe flux must be decreasing at lower altitudes, while the upgoing HF suprathermal electron flux must be decreasing as altitude increases above the HF-accelerated-electron source region near 250 km. These observed flux attenuations over ~50 km across H_{max} are entirely reasonable [*Abreu and Carlson*, 1977; *Carlson et al.*, 1982].

The conjugate photoelectron flux contributes to excitation of PLs across the full ionosphere above Arecibo. As illustrated in Figure 10, there is an additional contribution of HF-accelerated electron excitation of PLs only within the cylinder defined by the nominally circular disk from which HF suprathermal electrons stream up and down from the instability region near the height of HF reflection at 249 km for the time of this 4 min data segment. The ratio of the HF-enhanced PL intensities kT_p to kT_{pe} across the boundary is seen to fall from ~4 to ~1 $\pm$ ~0.2. The ISR diagnostic beam detects none of the upgoing (or backscattered downgoing) HF-accelerated electrons above 330 km for reasons of pure geometry. The ISR line-of-sight beam is looking along a 10.5° zenith angle, while the HF electron beam is near a 45° angle to vertical. Above ~330 km the ISR diagnostic beam is then cutting across magnetic field lines which do not trace back to the "instability source disk" from which the HF suprathermal electrons stream. That ratio above ~330 km in Figure 12 is unity within the standard deviation of the measurement confirms expectation. The sharp edge of HF-accelerated suprathermal electron flux is expected from the sharp cutoff of instabilities where the HF electric field drops below the instability threshold, as confirmed by in situ measurements by satellites at Arecibo [*Farley et al.*, 1983] and EISCAT Tromsø rockets [*Rose et al.*, 1985].

3.3. Comparison of Solar-Produced Versus HF-Produced Suprathermal Electron Fluxes

Having targeted conditions of weak suprathermal electron fluxes and weak HF-enhanced PLs, we are enabled to look at Figure 12 within the context of equation (3). Recall, by following the approach
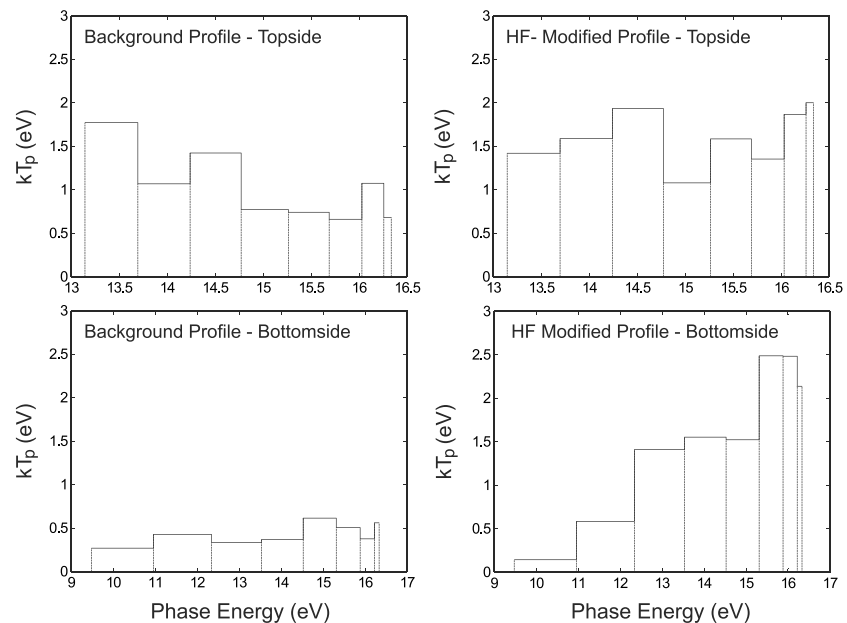
Figure 12. kT_p (eV) versus phase energy for profiles of left-topside and left-bottomside, respectively, topside and bottomside background (HF off) conditions, right-topside and right-bottomside for HF on conditions. The right-hand pair is thus the sum of the (unchanged) conjugate pe component plus the HF-accelerated suprathermal electrons. The difference between the HF off versus HF on is thus the suprathermal flux accelerated by high-power HF processes. This difference is observed to be a kT_p intensity of ~1 eV on the bottomside where the HF flux originates. Attenuation diminishes this to ~0.5 on the topside.

introduced in *Carlson et al.* [2015] as described here in section 3.1, we can use the ratios of kT_p/kT_e as a good linear approximation of the weak HF-accelerated suprathermal electron fluxes. We have in effect gone directly to comparison of solar pe versus HF-accelerated suprathermal electrons. Visual inspection alone, of Figure 8, gives an immediate feel for their comparability. Figure 10 quantifies this and does so with high precision and accuracy.

As discussed in *Carlson et al.* [1982] based simply on collision cross sections, elastic collisions approximately 10 times those of inelastic lead the HF-accelerated fluxes of approximately tens of eV to recover isotropy of direction between the inelastic collisions in which energy is lost. Mean free paths and columnar content (mainly atomic oxygen above 250 km here) thus confine significant interaction of the incoming suprathermal electrons to within about a neutral scale height of the height of unity optical depth. Downgoing photoelectrons (pe) as well as HF-accelerated suprathermal electrons accumulate a ratio of about 2 to 1 for downward to upward backscattered. The conjugate pe are incoming to the topside from the conjugate ionosphere (with some backscatter as described just below); the HF-accelerated suprathermals stream both upward and downward out from the thin HF acceleration slab. The added HF-accelerated electron flux component is quickly in quasi steady state. The added downgoing HF suprathermals parallel the same transport physics as the incoming conjugate pe; the upgoing HF suprathermal transport parallels the "backscattered" conjugate pe (including escape to the conjugate region). The primary difference lies in the source region (energy ranges are comparable).

At Arecibo in winter during local darkness and conjugate sunlit conditions, the incoming (downgoing) conjugate-source photoelectron flux is about triple the "reflected" pe flux going back up [*Mantas et al.*, 1978]. We use the terms "escape flux" from the conjugate ionosphere and "reflected component of suprathermal flux" in the sense of common usage, recognizing that as *Mantas et al.* [1978] explain in detail, this terminology is a simplification of the realities of steady state altitude-dependent pe fluxes along magnetic field lines. The HF-accelerated suprathermal electrons are "escaping" upward and downward from a relatively narrow (much less than a neutral scale height) altitude range.

Now we are ready to compare the magnitude of the HF-accelerated suprathermal electron flux with that of the conjugate pe flux arriving at the local topside ionosphere. We have chosen a time when there are

Table 1. Key Parameters for Two HF Electron Acceleration Experiments

Parameter	20 May 1972	11 November 2015
T_e enhancement	100–200 K	100–200 K
$T_e \sim T_i \sim T_n$ HF off	875 K (275 km)	910 K (280 km)
Doppler downshift	Upgoing suprath.	Upgoing suprath.
kT_p (eV)	~1 (~15 eV)	~1 (15 eV)
Altitude range	250–275 km	(250–275 and 295–320 km)
HF power (O mode)	138 kW (7.63 MHz)	6 × 75 kW (5.095 MHz)
f_oF_2	~8 MHz	6.8 MHz

no locally produced pe (winter far after local sunset) and a time when both the HF and conjugate pe fluxes are sufficiently weak that the measured kT_p are simply linearly proportional to the HF-accelerated or pe fluxes.

We have shown in the discussion of Figure 8 data that with the HF on, the bottomside kT_p excited by upgoing suprathermal electrons was 4 times that excited with the HF off. Thus, upgoing suprathermal fluxes excited by the sum of HF plus upgoing conjugate pe were 4 times those from upgoing conjugate pe alone. HF-produced upgoing suprathermal flux was 3 times that of the upgoing conjugate pe at this time. We know that the ratio of incident to backscatter on the order of tens eV suprathermal electrons is 2:1 [*Carlson et al.*, 1982]. We found here in our discussion the data shown in Figure 8 that the conjugate pe flux incident on the topside local ionosphere (~340 km) was measured here to be attenuated to ~1/3 that flux reaching the bottomside (~265 km). Therefore, the HF flux upgoing HF-excited flux is (4 × ½ × 1/3) = 2/3 the pe flux incident from the conjugate ionosphere at this time.

3.4. Efficiency of Energy Conversion for HF-Produced Suprathermal Electron Fluxes

The previous experiment leading to an estimate of order 10% efficiency [*Carlson et al.*, 1982; *Carlson*, 1993] detailed the process, subsequently used in *Pedersen et al.* [2009], and we follow the same process here. At this point let us start by comparing the ionospheric conditions, HF power, and experimental results (in particular measured values of kT_p) for the previous versus current experiment, summarized in Table 1 below.

Comparing the key parameters for the experimental implementation and the values of the observed HF effects, the conditions for the two experiments are strikingly similar. The only notable difference is the HF power density: May 1972 138 kW at 7.63 MHz versus November 2015 at 450 kW at 5.095 MHz, which would make the HF power aperture 45% stronger for the 11 November experiment. This would lead one to anticipate that kT_p for the HF-produced flux on the corresponding date would be ~45% greater for all else the same, within uncertainties of experimental measurement and reproducibility of relevant geophysical conditions and driving physics.

In Figure 12, we show the quantitative data leading to the kT_p for 11 November 2015 in the summary Table 1 and leading to our conclusion. Figure 12 shows PL (downshifted) intensity kT_p (eV) driven by upgoing suprathermal electrons versus phase energy. It shows the observed kT_p on the topside and bottomside ionosphere respectively in the top and bottom pair of plots and observed kT_p for the background (HF off) versus HF on conditions, respectively, in the left-hand versus right-hand pair of plots. The background kT_p is excited by only pe incoming from the conjugate sunlit hemisphere (overhead is in full local winter darkness). Since lowest-phase energy is sampled at lowest N_e, topside and bottomside phase energy profiles converge toward highest energies at H_{max}. We observe here that the conjugate pe flux incident on the topside local ionosphere near 340 km attenuates as it penetrates increasingly deeply. The conjugate pe flux incident on the topside yields a kT_p intensity ~1.3 eV, attenuating to an intensity ~0.4 eV on penetrating to ~260 km (attenuation consistent with *Abreu and Carlson* [1977] observations and *Schunk and Hays* [1971] theory). Turning HF on produces an upgoing suprathermal flux, adding ~1.1 eV to the background kT_p. This HF-accelerated upgoing suprathermal flux is thus comparable to the incoming conjugate pe flux at this 90° conjugate SZA. Scaling corrects that HF kT_p 1.1 eV measures upgoing suprathermals, while the conjugate kT_p 1.3 measure backscattered pe for which the forward to backscatter ratio is ~2:1 [*Carlson et al.*, 1982]. We chose to work with weak suprathermal fluxes to make kT_p linearly directly proportional to suprathermal electron flux. The radar wavelength and plasma frequency lead the particle energy sampled to be near and above 15 eV.

We have focused on the vicinity of ~15 eV for the juxtaposition of four reasons related to the HF-modified electron energy distribution. From the modeling perspective, *Gurevich et al.* [2004] with more focus on plasma physics have applied a kinetic theory conserving energy that predicts the growth with time of a high energy tail; *Gustavsson and Eliasson* [2008] with more focus on the aeronomy have shown the impact of vibrational excitation of N_2 important at lower altitudes; the latter introduces a "kink" in the slope of the energy distribution below 10 eV, but for energies above 10 eV the two approaches give similarly steady slopes to the electron energy distribution. Below 10 eV the role of electron energy losses to ambient electrons is strong, but that N_e dependence becomes weak by ~15 eV and above [*Schunk and Hays*, 1971; *Abreu and Carlson*, 1977]. The ISR PL radar wavelength at Arecibo's 430 MHz senses electrons in an N_e-dependent energy range of ~10–60 eV but is sensitive the energies in the 10–20 eV range long into the night; PL phase energies ~15 eV are most sensitive to particle energies near and above 15 eV. The threshold for electron impact-ionization of thermosphere constituents is within a few eV of 15 eV. The advantages of these theoretical, geophysical, and technical reasons merge to endorse the energy range we select.

While we have started here with noting a variety of self-consistency details, the primary point of Figure 12 is the magnitude of the kT_p attributed to the HF-accelerated suprathermal flux. We observe from Figure 12 that this magnitude in kT_p is 1 eV, around a phase energy of ~15 eV, which corresponds to electron-particle kinetic energies at and above 15 eV. This magnitude 1 eV is to be compared with the 20 May 1972 data. Magnitudes shown from the kT_p values ~12–15 eV in Figure 1 of *Carlson et al.* [1982] are found to be of intensity ~1 eV. In short both are about 1 eV; i.e., both are about the same.

While we pointed out a difference in driving HF power density ~45%, this is easily within any reasonable uncertainties of experiment and geophysical/physical repeatability. Recall that our context is that an efficiency > ~30% would violate physics of aeronomy and an efficiency > ~1% would render the question near irrelevant.

The kT_p values for the new November 2015 experiment are the same 1 eV magnitude as for the 20 May 1972 experiment reduces the rest of the analysis to a previously solved problem. Repeating the same analysis as detailed in *Carlson et al.* [1982] (the same procedure as repeated by *Pedersen et al.* [2009] leads to the same estimate of ~10% efficiency). We should point out nonetheless major improvements in data error bars and time resolution for the 11 November 2016 data and significant improvement in simplicity of comparing suprathermal electron fluxes. Here we have tailored the observations to (a) minimize uncertainties in interpretation of the data leading to the linear equation (3) versus the issues of the partial differential equation (2) and (b) allow direct comparison of solar-produced versus HF-acceleration produced suprathermal electrons. Similar observations were made a day before and 2 days after the 11 November 2015 data presented here to confirm repeatability. In short, the measured absolute kT_p intensities confirm repeatability of the initial ~10% efficiency in *Carlson* [1993], for midlatitudes (magnetic dip angle ~45°).

In contrast to section 3.3 where our point was to compare the HF-accelerated suprathermal electron flux to solar-produced pe fluxes, our point in section 3.4 has been to compare efficiency of conversion of HF radio wave energy to suprathermal electron flux kinetic energy. Here we have shown that the efficiency of this conversion is ~10% in this November 2015 experiments (an experiment running three nights), the same as it was in 1972. This then corroborates the conclusion in *Carlson* [1993] that high-power HF radio waves are a viable approach to producing near-Earth space plasmas or ionospheres, whether midlatitude of high latitude. Since *Pedersen et al.* [2009, 2010] showed ~10% conversion efficiency at HAARP, both physical regimes are accounted for.

4. Discussion

Entirely independent observations years apart, but under very similar ionosphere and experimental conditions, have shown repeatable ~10% HF conversion efficiencies of HF wave energy to accelerated electron kinetic energy at Arecibo. The original 1982 estimate of ~10% for conversion efficiency from radio wave to accelerated electron flux is substantiated by these new experiments in November 2015.

Major improvements in data quality and control conditions enabled for the first time:

1. Experimental design to observe low values of kT_p, removing self-damping effects on PL intensities, to enable direct comparisons of HF to solar suprathermal electrons.

2. Direct visual raw data comparison of PL excited by HF-accelerated suprathermal electrons versus solar-produced pe, making their comparability directly apparent.
3. Direct quantification of kT_p/kT_e ratios, removing complications of intermediate derivation of full quantitative pe specta, to quantify this "direct" comparison.
4. Direct observation of HF-accelerated suprathermal electron fluxes comparable to those from the conjugate solar-produced pe flux around 90° SZA (solar zenith angle) there.
5. Integration times reduced from former fraction of an hour to approximately a minute (a time resolution reducing changes with SZA to negligible levels.)

The suggestion that HF production of ionization could become competitive with that from the Sun was initially done with indirect calculations. These new data/techniques enable comparison for the first time with minimum (far fewer) theoretical intermediate steps.

Important context is that an efficiency greater than ~30% would violate physics of basic aeronomy [*Carlson and Jensen*, 2015]. This ~30% upper bound is due to the energy lost to by-products in the course of electron impact ionization producing a free electron. Approaching 30% is a very high efficiency. At the other end, less than ~1% efficiency would make the question more of academic than practical interest. Even highly conservative estimates of uncertainty in transmitter power and ionosphere absorption place the efficiency well within this range. Thus, the ~10% efficiency found makes the derived conversion efficiency of significant scientific and potentially practical interest.

We have emphasized, in section 2.4, three critical nonlinear phenomena confined to high latitudes: (1) the Figure 3 "HF trapping" dependence on the HF propagation angle to **B**, (2) the dependence on the angle to **B** of the direction of the HF **E** vector, and (3) the dramatic amplification of the HF power (hence of plasma heating and electron acceleration) due to pointing the line of sight of the HF transmitter in the direction parallel to **B**. This discovery has come to be called the magnetic zenith effect [*Gurevich et al.*, 2001]. Figure 3 of *Gurevich et al.* [2002] illustrates the HF power amplification factor in magnetic zenith. In addition, the amplification for HF operations at multiples of the electron gyroharmonic frequency is also well documented at high latitudes [e.g., *Djuth et al.*, 2005; *Blagoveshchenskaya et al.*, 2009; *Grach et al.*, 2014]. The compound effect is major. None of these four amplifications can apply here to Arecibo. Comparable ~10% efficiencies at both Arecibo and HAARP thus mean something else are offsetting what would otherwise seem to bias high efficiencies to high latitude versus midlatitude. Indeed, we have noted near the end of section 2.4 that the angle of the HF **E** to Earth's magnetic field **B** determines the instability growth rate and ultimate amplitude and, for example, at 8.175 MHz, the HF power for **E** perpendicular to **B** at HAARP is 45%, while at Arecibo it is ~1.5%. The energy deposition per unit time as the HF radio waves pass through the UH region at Arecibo is thus concluded to be minimal en route to reaching the altitude at which the Langmuir decay instability can dominate [e.g., *Djuth and Dubois*, 2015].

The low-latitude conversion efficiency is so comparable to that at high latitudes, despite the significant advantage of known processes dominating high latitudes, raises the issue of a fundamental role for suprathermal electrons in transporting energy out of plasma instability regions, beyond the details of which particular instability may dominate which conditions. The latter depends on competition among various instabilities of different growth rates. The former is more about the fundamental balance between incident wave energy driving instabilities, and particle kinetic energy carried away by accelerated electrons.

For O-mode HF transmissions, the early time acceleration of electrons in the plasma arises because of the generation and collapse of Cavitons near the critical layer. Early time refers to 10–100 ms after HF turn-on depending on *E*-region conductivity, which determines the rate of HF irregularity formation. Once large-scale irregularities form it is difficult to track the Cavitons with radar. The modified/extended Zakharov model of *DuBois et al.* [1988, 1990, 1993, 2001] has been successful in predicting the details of the Caviton formation and identifying what the early time HF-enhanced plasma line/ion line spectral signatures should be. These spectral signatures were subsequently observed at Arecibo and Tromsø [*Sulzer and Fejer*, 1994; *Isham et al.*, 1999; *Rietveld et al.*, 2000; *Cheung et al.*, 2001; *Djuth et al.*, 2004]. As discussed in *Djuth and DuBois* [2015], Cavitons are localized states of Langmuir oscillations. The longitudinal electric field envelope of the Langmuir field is trapped in a local depression in the electron density, or cavity, thus the name "caviton." When the trapped Langmuir field is resolved in spatial Fourier modes the frequencies of these modes of the localized state lie below the free Langmuir wave dispersion curve, usually even below the local electron

plasma frequency. Therefore, these states cannot be represented as a wave packet of free Langmuir waves; Cavitons are an emergent nonlinear phenomenon. The localized Langmuir wave electric field exerts a ponderomotive force, which tends to reduce the local electron density, which in turn localizes the field even more and lowers the frequencies further below the electron plasma frequency. This structure tends to collapse to smaller scales as first predicted by *Zakharov* [1972]. The details of the collapse process depend on the spatial dimension of the theory or simulation and the method of driving. As the spatial scale decreases, and higher wave numbers are excited in the Fourier spectrum, the Langmuir electric field is quenched by a form of collisionless Landau damping that generates suprathermal electrons. This leaves behind a density cavity with no trapped electric field, a result called "burnout." The burnt out density cavities can then be the nucleation centers for new cavitons with localized electric fields.

Suprathermal electrons produced by Caviton burnout recirculate through the production region because of elastic electron collisions that occur outside the region [e.g., *Carlson et al.*, 1982; *Gurevich et al.*, 1985, 2000]. According to *Carlson et al.* [1982], "the suprathermal electrons have a mean free path of several kilometers and suffer about 10 elastic collisions before each inelastic collision. No matter what the acceleration mechanism is, elastic collisions serve to rapidly fill in loss cones." Thus, a more complete description of the modification process requires that successive turbulent layers be tied together because they are linked by downgoing and upcoming fluxes of suprathermal electrons. This can only be accomplished with a purely kinetic simulation model. The ubiquitous generation of suprathermal electrons from Langmuir turbulence created by parametric instabilities has led to the development of new kinetic modeling tools, which can be applied to HF ionospheric modification phenomena. Considerable progress has been made in laser–plasma modeling. One model called the Quasilinear Zakharov model [*Sanbonmatsu et al.*, 2000; *Myatt et al.*, 2013] can model 10 km or greater plasma layers near HF reflection in 2-D simulations and hundreds of meters in 3-D simulations with current parallel computing capabilities. Theoretical studies of late time phenomena [*Gurevich et al.*, 2004] and work related to the HAARP ionization layers [*Eliasson et al.*, 2012; *Mishin et al.*, 2016] have aided our understanding of the interaction of suprathermal electrons with the ionosphere. However, the detailed physics behind the electron acceleration at late times greater than ~10 ms at Arecibo remains somewhat elusive. In addition, it is unclear how acceleration occurs in the presence of filamentary irregularity structures that dominate the Arecibo plasma beginning 20 to 40 s after HF turn-on in unmodified background plasma. The late time development of suprathermal electrons will be the focus of future experiments at Arecibo.

5. Conclusions

The efficiency of conversion of HF radio wave energy to accelerated electron kinetic energy is a critical parameter in determining the practicality of production of ionospheric plasma from the ground. The crucial step in this conversion is acceleration of electrons to suprathermal energies of at least several tens of eV and dominate ion production. The ~10% HF conversion efficiency for ionization production found over 20 years ago [*Carlson*, 1993] is confirmed here as a repeatable value. Thus, production of ionization from the ground is confirmed to be practicable at midlatitudes, such as Arecibo, as well as high latitudes. We have also shown direct comparison of HF-produced suprathermal electron fluxes relative to solar produced pe fluxes.

The same conversion efficiency ~10% is comparable at midlatitude Arecibo as well as at high-latitude HAARP [*Pedersen et al.*, 2009] is significant, given the fundamental differences in physical processes dominating the overall physics at high latitudes versus lower-middle latitudes. All the more so given that it is specific different instability processes which dominate in these different latitude ranges. The physical process at Arecibo is dominated here by the Langmuir decay instability operating near the height of HF reflection. This is in contrast to at high latitudes dominated by four entirely different physical processes, which compound to yield a similar ~10% efficiency of wave to particle energy conversion, but at an altitude a few kilometer below that which dominates the Arecibo midlatitude environment. Understanding of both is needed.

Accelerated electrons are so important to dissipation of energy deposited by instabilities driven by large electric fields, under these diverse plasma conditions, which suggest that electron acceleration may play a more fundamental role in energy distribution in plasmas than generally recognized.

In short we have confirmed 10% energy conversion efficiency for HF radio wave to kinetic electron acceleration, based on PL intensity measurements. We have substantiated that HF radio waves can create space

plasmas at both middle and high latitudes, including directly showing ratios of HF accelerated to solar photoelectrons. Generalizing our findings supports the speculation that electron acceleration may be more essential to distribution of energy in space plasmas than recognized.

References

Abreu, V. J., and H. C. Carlson (1977), Photoelectron energy loss and spectral features deduced by the plasma line technique, *J. Geophys. Res.*, *82*, 1017–1023, doi:10.1029/JA082i007p01017.

Bernhardt, P. A., C. A. Tepley, and L. M. Duncan (1988), Artificial airglow excited by high-power radio waves, *Science*, *242*, 1022–1027, doi:10.1126/science242.4881.1022.

Blagoveshchenskaya, N. F., H. C. Carlson, V. A. Konienko, T. D. Borisova, M. T. Rietveld, T. K. Yeoman, and A. Brekke (2009), Phenomena induced by powerful HF pumping towards magnetic zenith with a frequency near the F-region critical frequency and the third electron gyro harmonic frequency, *Ann. Geophys.*, *27*, 131–145, doi:10.5194/angeo-27-131-2009.

Carlson, H. C. (1987), Artificial ionosphere—Creation using high power HF transmitters AFGL1987/ILIR7L, AFGL)PL/CAG), Hanscom AFB, Mass.

Carlson, H. C. (1990), High Power HF Modification: Geophysics AGARD EPP Symposium Proceedings, 1B, 1-13.

Carlson, H. C. (1993), High power HF modification-geophysics, span of EM effects, and energy budget, *Adv. Space Res.*, *13*, 1015–1024, doi:10.1016/0273-1177(93)90046-E.

Carlson, H. C., and J. B. Jensen (2015), HF accelerated electron fluxes, spectra, and ionization, *Earth Moon Planets*, *116*, 1–18, doi:10.1007/s11038-014-9454-6.

Carlson, H. C., W. E. Gordon, and R. L. Showen (1972), High frequency induced enhancements of the incoherent scatter spectrum at Arecibo, *J. Geophys. Res.*, *77*, 1242–1250, doi:10.1029/JA077i007p01242.

Carlson, H. C., V. B. Wickwar, and G. P. Mantas (1977), The plasma line revisited as an aeronomical diagnostic: Suprathermal electrons, solar EUV, electron gas thermal balance, *Geophys. Res. Lett.*, *4*, 565–567, doi:10.1029/GL004i012p00565.

Carlson, H. C., V. B. Wickwar, and G. P. Mantas (1982), Observations of fluxes of suprathermal electrons accelerated by HF excited instabilities, *J. Atmos. Terr. Phys.*, *44*, 1089–1100, doi:10.1016/0021-9169(82)90020-4.

Carlson, H. C., K. Oksavik, and J. I. Moen (2013), Thermally excited 630.0 nm O(1**D**) emission in the cusp: A frequent high-altitude transient signature, *J. Geophys. Res. Space Physics*, *118*, 5842–5852, doi:10.1002/jgra.50516.

Carlson, H. C., F. T. Djuth, P. Perillat, and M. Sulzer (2015), Low latitude 10 eV electrons: Nighttime plasma line as a new research capability, *Geophys. Res. Lett.*, *42*, 7255–7263, doi:10.1002/2015GL065172.

Cheung, P. Y., M. P. Sulzer, D. F. DuBois, and D. A. Russell (2001), High-power high-frequency-induced Langmuir turbulence in a smooth ionosphere at Arecibo. II. Low duty cycle, altitude-resolved, observations, *Phys. Plasmas*, *8*, 802–812, doi:10.1063/1.1345704.

Cicerone, R. J. (1974), Photoelectrons in the ionosphere: Radar measurements and theoretical computations, *Rev. Geophys. Space Phys.*, *12*, 259–271, doi:10.1029/RG012i002p00259.

Djuth, F. T., and D. F. Dubois (2015), Temporal development of HF Langmuir and ion turbulence at Arecibo, *Earth Moon Planets*, doi:10.1007/s11038-015-9458-x.

Djuth, F. T., et al. (1999), Large airglow enhancements produced via wave-plasma interactions in sporadic E, *Geophys. Res. Lett.*, *26*, 1557–1560, doi:10.1029/1999GL900296.

Djuth, F. T., B. Isham, M. T. Rietveld, T. Hagfors, and C. La Hoz (2004), The first 100 ms of HF modification at Tromsø, Norway, *J. Geophys. Res.*, *109*, A11307, doi:10.1029/2003JA010236.

Djuth, F. T., T. R. Pedersen, E. A. Gerkin, P. A. Bernhardt, C. A. Selcher, W. A. Bristow, and M. J. Kosch (2005), Ionospheric modification at twice the electron cyclotron frequency, *Phys. Res. Lett.*, *94*, 125,001–125,004, doi:10.1103/PhysRevLett.94.125001.

DuBois, D. F., H. A. Rose, and D. Russell (1988), Power spectra of fluctuations in strong Langmuir turbulence, *Phys. Rev. Lett.*, *61*, 2209–2212, doi:10.1103/PhysRevLett.61.2209.

DuBois, D. F., H. A. Rose, and D. Russell (1990), Excitation of strong Langmuir turbulence in plasmas near critical density: Application to HF heating of the ionosphere, *J. Geophys. Res.*, *95*, 21,221–21,272, doi:10.1029/JA095iA12p21221.

DuBois, D. F., A. Hanssen, H. A. Rose, and D. Russell (1993), Space and time distribution of HF excited Langmuir turbulence in the ionosphere: Comparison of theory and experiment, *J. Geophys. Res.*, *98*, 17,543–17,567, doi:10.1029/93JA01469.

DuBois, D. F., D. A. Russell, P. Y. Cheung, and M. P. Sulzer (2001), High-power high-frequency-induced Langmuir turbulence in a smooth ionosphere at Arecibo. I. Theoretical predictions for altitude-resolved plasma line radar spectra, *Phys. Plasmas*, *8*, 791–801, doi:10.1063/1.1345703.

Eliasson, B., X. Shao, G. Milikh, E. V. Mishin, and K. Papadopoulos (2012), Numerical modeling of artificial ionospheric layers driven by high-power HF heating, *J. Geophys. Res.*, *117*, A10321, doi:10.1029/2012JA018105.

Farley, D. T., C. LaHoz, and B. G. Fejer (1983), Studies of the self-focusing instability at Arecibo, *J. Geophys. Res.*, *88*, 2093–2102, doi:10.1029/JA088iA03p02093.

Franz, T. L., M. C. Kelley, and A. V. Gurevich (1999), Radar backscattering from artificial field-aligned irregularities, *Radio Sci.*, *34*, 465–475, doi:10.1029/1998RS900035.

Fremouw, E. J., J. Petriceks, and F. W. Perkins (1969), Thomson scatter measurements and magnetic field effects on the Landau damping and excitation of plasma waves, *Phys. Fluids*, *12*, 869–874, doi:10.1063/1.1692569.

Gordon, W. E., and H. C. Carlson (1974), Arecibo Heating Experiments, *Radio Sci.*, *9*, 1041–1047, doi:10.1029/RS009i011p01041.

Grach, S. M., E. N. Sergeev, A. V. Shindin, E. V. Mishin, and B. Watkins (2014), Artifical ionosphere layers for pumping-wave frequencies near the fourth electron gyroharmonic in experiments at HAARF facility, *Dokl. Phys.*, *59*, 62–66, doi:10.1134/S1028335814020074.

Gurevich, A., H. C. Carlson, A. V. Lukyanov, and K. P. Zybin (1997), Parametric decay of upper hybrid plasma waves trapped inside density irregularities in the ionosphere, *Phys. Lett. A*, *231*, 97–108, doi:10.1016/S0375-9601(97)00282-X.

Gurevich, A., T. Hagfors, H. C. Carlson, A. Karashin, and K. P. Zybin (1998), Self-oscillations and bunching of striations in ionospheric modifications, *Phys. Lett. A*, *239*, 385–392, doi:10.1016/S0375-9601(98)00006-1.

Gurevich, A., H. C. Carlson, M. Kelley, T. Hagfors, A. Karashtin, and K. Zybin (1999), Nonlinear structuring of the ionosphere modified by powerful radio waves at low latitudes, *J. Phys. Lett. A*, *251*, 311–321, doi:10.1016/S0375-9601(98)00786-5.

Gurevich, A. V. (2007), Nonlinear effects in the ionosphere: Reviews of topical problems, *Phys.-Usp.*, *50*(11), 1091–1121 PACS 41.20. Jb,52.35-g.52.40.Db, 94.20-y, doi:10.1070/PU2007v050n11ABEH006212.

Gurevich, A. V., I. S. Dimant, G. M. Milikh, and V. V. Vas'kov (1985), Multiple acceleration of electrons in the regions of high-power radio-wave reflection in the ionosphere, *J. Atmos. Terr. Phys.*, *47*, 1057–1070, doi:10.1016/0021-9169(85)90023-6.

Gurevich, A. V., A. V. Lukyanov, and K. P. Zybin (1995), Stationary state of isolated striations developed during ionospheric modification, *Phys. Lett. A*, *206*(3), 247–259, doi:10.1016/0375-9601(95)00595-T.

Gurevich, A. V., H. C. Carlson, G. M. Milikh, K. P. Zybin, F. T. Djuth, and K. M. Groves (2000), Suprathermal electrons generated by the interaction of a powerful radio wave with the ionosphere, *Geophys. Res. Lett.*, *27*, 2461–2464, doi:10.1029/2000GL003770.

Gurevich, A. V., H. C. Carlson, and K. P. Zybin (2001), Nonlinear structuring and southward shift of a strongly heated region in ionospheric modification, *Phys. Lett. A*, *288*, 231–239, doi:10.1016/S0375-9601(01)00516-3.

Gurevich, A. V., K. P. Zybin, H. C. Carlson, and T. Pedersen (2002), Magnetic zenith effect in ionospheric modifications, *Phys. Lett. A*, *305*, 264–274, doi:10.1016/S0375-9601(02)01450-0.

Gurevich, A. V., H. C. Carlson, Y. V. Medvedev, and K. P. Zybin (2004), Langmuir turbulence in ionospheric plasma, *Plasma Phys. Rep.*, *30*(12), 995–1005, doi:10.1134/1.1839953.

Gurevich, A. V., K. P. Zybin, and H. C. Carlson (2005), Magnetic-zenith effect, *Radiophys. Quantum Electron.*, *48*(9), 686–699, doi:10.1007/s11141-005-0113-7.

Gustavsson, B., and B. Eliasson (2008), HF radio wave acceleration of ionospheric electrons: Analysis of HF-induced optical enhancements, *J. Geophys. Res.*, *113*, A08319, doi:10.1029/2007JA012913.

Gustavson, B., T. B. Lyser, M. Kosch, M. T. Reiyveld, A. Steen, B. U. E. Brandstrom, and T. Aso (2006), Electron gyroharmonic effects in ionization and electron acceleration during high-frequency pumping in the ionosphere, *Phys. Rev. Lett.*, *97*, 195002, doi:10.1103/physrevlett.97.195002.

Hysell, D. L., R. H. Varney, M. N. Vlasov, E. Nossa, B. Watkins, T. Pedersen, and J. D. Huba (2012), Estimating the electron energy distribution during ionospheric modification from spectrographic airglow measurements, *J. Geophys. Res.*, *117*, A02317, doi:10.1029/2011JA017187.

Hysell, D. L., R. J. Miceli, E. A. Kendall, N. M. Schlatter, R. H. Varney, B. J. Watkins, T. R. Pedersen, P. A. Bernhardt, and J. D. Huba (2014), Heater-induced ionization inferred from spectrometric airglow measurements, *J. Geophys. Res. Space Physics*, *119*, 2038–2045, doi:10.1002/2013JA019663.

Isham, B., C. La Hoz, T. B. Leyser, M. T. Rietveld, and T. Hagfors (1999), Cavitating Langmuir turbulence observed during high-latitude ionospheric wave interaction experiments, *Phys. Rev. Lett.*, *83*, 2576–2579, doi:10.1103/PhysRevLett.83.2576.

Kantor, I. J. (1974), High frequency induced enhancements of the incoherent backscatter spectra at Arecibo, 2, *J. Geophys. Res.*, *79*, 199–208, doi:10.1029/JA079i001.

Kelley, M. C., T. L. Arce, J. Salowey, M. Sulzer, T. Armstrong, M. Carter, and L. Dunkin (1995), Density depletions at the 10-m scale induced by the Arecibo heater, *J. Geophys. Res.*, *100*, 17,367–17,376, doi:10.1029/95JA00063.

Kosch, M. J., M. T. Rietveld, T. Hagfors, and T. B. Leyser (2000), High-latitude HF induced airglow displaced equatorwards of the pump beam, *Geophys. Res. Lett.*, *27*(17), 2817–2820, doi:10.1029/2000GL003754.

Mantas, G. P. (1973), Electron collision processes in the ionosphere PhD thesis, Univ. of Illinois, Urbana.

Mantas, G. P. (1975), Theory of photoelectron thermalization and transport in the ionosphere, *Planet. Space Sci.*, *23*, 337–352, doi:10.1016/0032-0633(75)90139-7.

Mantas, G. P. (1994), Large 6300-Å airglow intensity enhancements observed in ionosphere heating experiments are excited by thermal electrons, *J. Geophys. Res.*, *99*, 8993–9002, doi:10.1029/94JA00347.

Mantas, G. P., and H. C. Carlson (1991), Reexamination of the 0(3p- > 1D) excitation rate by thermal electron impact, *Geophys. Res. Lett.*, *18*, 159–162, doi:10.1029/91GL00019.

Mantas, G. P., V. B. Wickwar, and H. C. Carlson (1975), Plasma line and theoretical studies of photoelectrons at Arecibo, *Eos Trans. AGU*, *56*, 1037.

Mantas, G. P., H. C. Carlson, and V. B. Wickwar (1978), Photoelectron flux build-up in the plasmasphere due to collisional backscatter from the ionosphere, *J. Geophys. Res.*, *83*, 1–15, doi:10.1029/JA083iA01p00001.

Mishin, E., B. Watkins, N. Lehtinen, B. Eliasson, T. Pedersen, and S. Grach (2016), Artificial ionospheric layers driven by high-frequency radiowaves: An assessment, *J. Geophys. Res. Space Physics*, *121*, 3497–3524, doi:10.1002/2015JA021823.

Myatt, J. F., H. X. Vu, D. F. DuBois, D. A. Russell, J. Zhang, R. W. Short, and A. V. Maximov (2013), Mitigation of two-plasmon decay in direct-drive inertial confinement fusion through the manipulation of ion acoustic and Langmuir wave damping, *Phys. Plasmas*, *20*, 052705, doi:10.1063/1.4807036.

Pedersen, T., B. Gustavsson, E. Mishin, E. MacKenzi, H. C. Carlson, M. Starks, and T. Mills (2009), Optical ring formation and ionization production in high power HF heating experiments at HAARP, *Geophys. Res. Lett.*, *36*, L18107, doi:10.1029/2009GL040047.

Pedersen, T., B. Gustavsson, E. Mishin, E. Kendall, T. Mills, H. C. Carlson, and A. L. Snyder (2010), Creation of artificial ionospheric layers using high power HF waves, *Geophys. Res. Lett.*, *37*, L02106, doi:10.1029/2009GL041895.

Pedersen, T. R., and H. C. Carlson (2001), First observations of HF heater-produced airglow at the high frequency active auroral research program facility: Thermal excitation and spatial structuring, *Radio Sci.*, *36*, 1013–1026, doi:10.1029/2000RS002399.

Pedersen, T. R., and E. A. Gerken (2005), Creation of visible artificial optical emissions in the aurora by high-power radio waves, *Nature*, *433*(7025), 498–500, doi:10.1038/nature03243.

Pedersen, T. R., M. McCarrick, E. Gerken, C. Selcher, D. Sentman, H. C. Carlson, and A. Gurevich (2003), Magnetic zenith enhancement of HF radio-induced airglow production at HAARP, *Geophys. Res. Lett.*, *30*(4), 1169, doi:10.1029/2002GL016096.

Pedersen, T. R., R. Esposito, M. Starks, and M. McCarrick (2008), Quantitative determination of HF radio-induced optical emission production efficiency at high latitudes, *J. Geophys. Res.*, *113*, A11316, doi:10.1029/2008JA013502.

Perkins, F. W., and E. E. Salpeter (1965), Enhancement of plasma density fluctuations by non-thermal electrons, *Phys. Rev.*, *139*, A55–A62, doi:10.1103/PhysRev.139.A55.

Rao, P. B., and G. D. Thome (1974), A model for RF scattering from field-aligned heater-induced irregularities, *Radio Sci.*, *9*, 987–996, doi:10.1029/RS009i011.

Rees, M. H., and D. Luckey (1974), Auroral electron energy derived from ratio of spectroscopic emission 1. Model computation, *J. Geophys. Res.*, *88*, 5181–5186, doi:10.1029/JA079i034p05181.

Rietveld, M. T., B. Isham, H. Kohl, C. La Hoz, and T. Hagfors (2000), Measurements of HF enhanced plasma and ion lines at EISCAT with high altitude resolution, *J. Geophys. Res.*, *105*, 7429–7439, doi:10.1029/1999JA900476.

Rietveld, M. T., M. J. Kosch, N. F. Blagoveshchenskaya, V. A. Kornienko, T. B. Leyser, and T. K. Yeoman (2003), Ionospheric electron heating, optical emissions, and striations induced by powerful HF radio waves at high latitudes: Aspect angle dependence, *J. Geophys. Res.*, *108*(A4), 1141, doi:10.1029/2002JA009543.

Rishbeth, H., and O. Garriott (1969), *Introduction to Ionospheric Physics*, Academic Press, New York.

Rose, G., B. Grandal, E. Neske, W. Ott, K. Spencer, J. Holtet, K. Masede, and J. Troim (1985), Experimental results from the HERO project: In situ measurements of ionospheric modifications using sounding rockets, *J. Geophys. Res.*, *90*, 2851–2860, doi:10.1029/JA090iA03p02851.

Sanbonmatsu, K. Y., H. X. Vu, B. Bezzerides, and D. F. DuBois (2000), The effect of kinetic processes on Langmuir turbulence, *Phys. Plasmas*, *7*, 1723–1731, doi:10.1063/1.873991.

Schunk, R. W., and P. B. Hays (1971), Photoelctron energy losses to thermal electrons, *Planet. Space Sci.*, *19*, 113, doi:10.1016/0032-0633(71)90071-7.

Showen, R. L. (1979), The spectral measurement of plasma lines, *Radio Sci.*, *14*, 503–508, doi:10.1029/RS014i003p00503.

Strickland, D. J., J. R. Jasperse, and J. A. Whalen (1983), Dependence of auroral FUV emissions on the incident electron spectrum and neutral atmosphere, *J. Geophys. Res.*, *88*, 8051–8062, doi:10.1029/JA088iA10p08051.

Sulzer, M. P. (1986), A radar technique for high range resolution incoherent scatter autocorrelation function measurements utilizing the full power of klystron radars, *Radio Sci.*, *21*, 1033–1040, doi:10.1029/RS021i006p01033.

Sulzer, M. P., and J. A. Fejer (1994), Radar spectral observations of HF-induced Langmuir turbulence with improved range and time resolution, *J. Geophys. Res.*, *99*, 15,035–15,050.

Utlaut, W. F., and R. Cohen (1971), Modifying the ionosphere with intense radio waves, *Science*, *174*, 245–254, doi:10.1126/science.174.4006.245.

Woods, T. N., et al. (2012), Extreme Ultraviolet Variability Experiment (EVE) on the Solar Dynamics Observatory (SDO): Overview of science objectives, instrument design, data products, and model developments, *Solar Phys.*, *275*, 115–143, doi:10.1007/s11207-009-9487-6.

Yngvesson, K. O., and F. W. Perkins (1968), Radar Thomson scatter studies of Photoelectrons in the ionosphere and Landau damping, *J. Geophys. Res.*, *73*, 97–110, doi:10.1029/JA073i001p00097.

Zakharov, V. E. (1972), Collapse of Langmuir waves, *Sov. Phys. JEPT, Eng. Transl.*, *35*, 908–920.